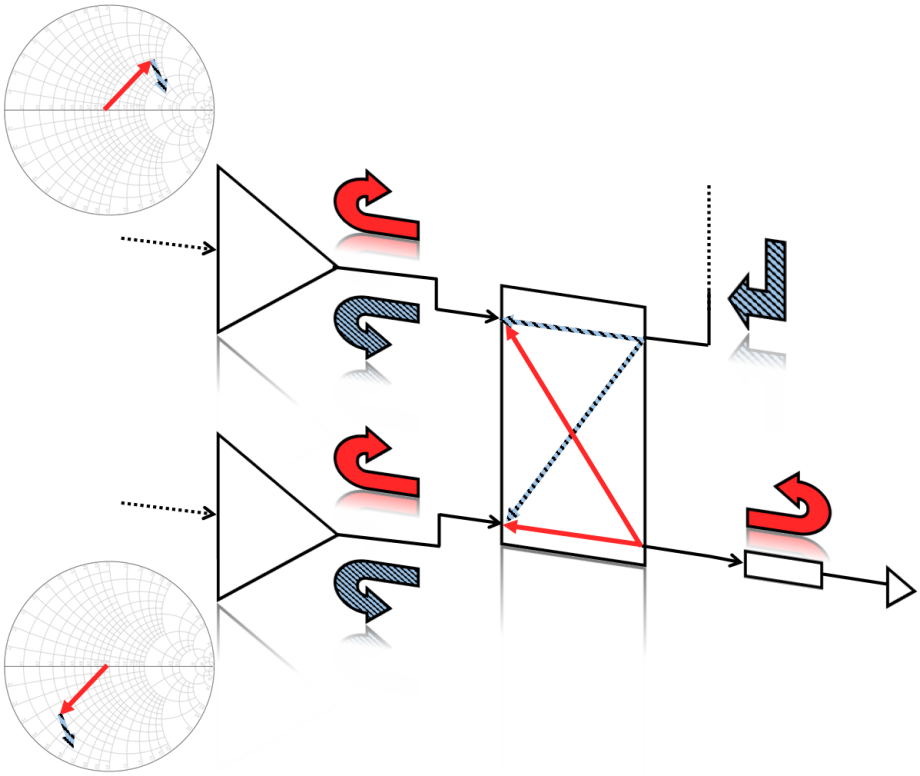

Possibilities of the LMBA in modern radar systems

An investigation of different load modulation techniques and their advantages

Master's thesis in Wireless, photonics and space engineering

Ludwig Gustavsson

DEPARTMENT OF MICROTECHNOLOGY AND NANOSCIENCE
CHALMERS UNIVERSITY OF TECHNOLOGY
Gothenburg, Sweden 2024
www.chalmers.se

Master's thesis 2024

Possibilities of the LMBA in modern radar systems

An investigation of different load modulation techniques and their advantages

LUDWIG GUSTAVSSON

CHALMERS
UNIVERSITY OF TECHNOLOGY

Department of Microtechnology and Nanoscience
Division of Microwave Electronics
Chalmers University of Technology
Gothenburg, Sweden 2024

Possibilities of the LMBA in modern radar systems
An investigation of different load modulation techniques and their advantages
LUDWIG GUSTAVSSON

Supervisor: Albin Nilsson, Saab AB
Examiner: Christian Fager, Department of Microtechnology and Nanoscience

Master's Thesis 2024
Department of Microtechnology and Nanoscience
Division of Microwave Electronics
Chalmers University of Technology
SE-412 96 Gothenburg
Telephone +46 31 772 1000

Cover: Working principle of the LMBA under effect of a mismatch (red arrow) and control signal (blue/striped arrow).

Typeset in LaTeX
Printed by Chalmers Reproservice
Gothenburg, Sweden 2024

Possibilities of the LMBA in modern radar systems
An investigation of different load modulation techniques and their advantages
LUDWIG GUSTAVSSON
Department of Microtechnology and Nanoscience
Chalmers University of Technology

Abstract

This master's thesis was performed in order to examine whether load modulation can be used in order to compensate for systems with reflections due to coupling between elements or poor output match. As these reflections worsen the performance of amplifiers, it is of great interest to mitigate these effects. An example of the implementation of this could be the AESA, where the reflections are dependent of the steering angle of the antenna. The proposed technique for compensation is the load modulated balanced amplifier (LMBA), where a control signal is injected at the isolated port of the second hybrid in a balanced amplifier (BA). In this report, four different topologies for this is assessed, where each uses a different way of injecting the control signal. These topologies are the LMBA, orthogonal LMBA (OLMBA), recursive LMBA (RLMBA) and reflective LMBA (RefLMBA). The load modulating techniques in these topologies are firstly examined by theoretically deriving how each topology is load modulated. This is then verified using non ideal components in the simulation software program Advanced Design Systems (ADS). As a last step, a BA is built with external components in order to verify the operation of the LMBA. The report finds that the theoretical equations for load modulation in an unmatched system shows the same characteristics as the simulation. Both the theory, simulations and measurements shows that the phase of the control signal has to be actively tuned in order to achieve the best load modulating behaviour. However, the load modulation is shown to yield better performance when properly tuned, even outside the bandwidth of the amplifier. This means that while load modulation can be used to compensate for reflections, the technique for which how this is done needs to be refined before it is ready to be implemented.

Keywords: Load modulation, LMBA, OLMBA, RLMBA, RefLMBA, PAE, AESA, Load-pull.

Acknowledgements

Although only my name is written as the author, there are a number of people who made this thesis work possible. Firstly, I would like to express my deepest appreciation to my supervisor Albin Nilsson for countless hours of great support, enthusiasm and ideas throughout this project. Secondly, I am extremely grateful to my examiner Christian Fager for his great advice, discussions and suggestions. Thirdly, I very much appreciate the help from Nicklas Billström, Theofilos Markopoulos and Klas Axelsson for the feedback and thoughts I have been given during the project. A special thanks also to Jörgen Andersson for his endless aid in designing the PCB, and to Daniel Carlsson who made sure that the PCB was producible. Even though the PCB was not used in this work, I highly value the experience of designing one. I would also like to extend my sincere thanks to Saab AB for offering me this thesis work. In particular Natalie Issa who set up this thesis work and helped me get started in my work, and Marie Ström who took up her torch and continued to be a great source of assistance. Lastly, I also had the great pleasure of working with the microwave design group at Saab, who have been both helpful and welcoming throughout the thesis.

Ludwig Gustavsson, Gothenburg, May 2024

List of Acronyms

Below is the list of acronyms that have been used throughout this thesis listed in alphabetical order:

ADS	Advanced design systems, a design program provided by Keysight
AESA	Active electronically scanned array
BA	Balanced Amplifier
Cal kit	Calibration kit
CS	Control signal
DUT	Device under test
GPIB	General purpose interface bus
LMBA	Load modulated balanced amplifier
OLMBA	Orthogonal load modulated balanced amplifier
PAE	Power added efficiency
PCB	Printed circuit board
RefLMBA	Reflective load modulated balanced amplifier
RF	Radio frequency
RLMBA	Recursive load modulated balanced amplifier
S-matrix	Scattering matrix
S-parameters	Scattering parameters
TRL	Through, reflect, line
VNA	Vector network analyser
QFN	Quad flat no-lead package

Contents

List of Figures

List of Tables

1
Introduction

In this chapter, a short theoretical- and practical background to the project will be given. This is followed by specifying the aim, limitations och issues that are being investigated.

1.1 Background

Even though wireless communication systems have been around for decades, there still exists a need to further develop this technology. This is a necessity in order to fulfil an increasing demand for larger data handling, as well as ensuring that modern technology reaches all corners of the world. Additionally, as more focus are put into creating a sustainable society, the big apparatus that builds our communication system has to be made more efficient. Within modern communication systems, there is a multitude of parameters that needs to be considered. Noise within the system has to be limited while maintaining a decent efficiency [2]. Then, the signal has to be of high enough power for the signal to reach its destination. Of course, there are many more parameters to take into account, but these are some of the more important when talking about amplifying elements in wireless systems [3].

The radio frequency (RF) amplifier is a versatile component as its function can be optimized for different applications. For instance are high linear output power, low noise and efficiency some of its key properties. Hence, it can be implemented as an amplifier before transmitting the signal, as a low-noise amplifier after receiving the signal and much more. In short, RF amplifiers are the cornerstone of communication systems. The wide span of implementations of RF amplifiers makes it easy to understand why it is the focus among many modern microwave researchers. However, the research is not only focused on communication systems, as low-noise amplifiers are vital for some quantum computers [4].

One of the latest additions to the RF amplifier topologies is the load modulated balanced amplifier (LMBA). This amplifier can be seen in Figure 1.1. The basic principle of the amplifier is the same as the balanced amplifier (BA), consisting of two 90° hybrids with two identical amplifiers in between. One of the benefits of this topology is that it makes the circuit more resilient to matching errors of the amplifier. Assuming that the two amplifiers have the same input impedance, their respective reflections will cancel each other out at the isolated port of the first hybrid [5, 6]. Now, by injecting a control signal into the isolated port of the second hybrid, the load that the amplifiers experience will change. Therefore, it is possible to tune the point of operation of the amplifiers, possibly yielding higher power added efficiency (PAE) and higher output power at back-off, while also providing a wider bandwidth of the amplifier [6].

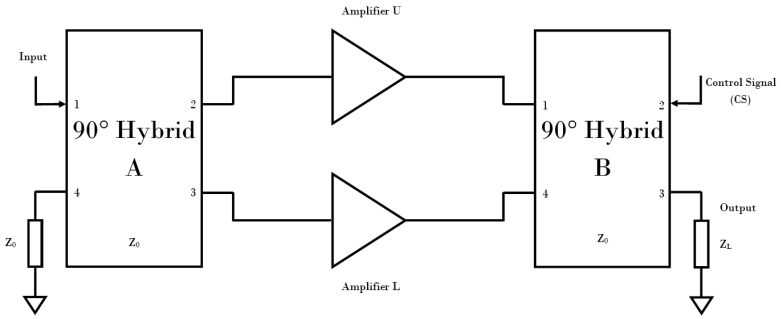

Figure 1.1: Basic structure of an LMBA amplifier.

This master thesis is offered by the microwave design team at Saab. The team works at the surveillance department of Saab, which focuses on modern radar systems for military applications. One of their areas of interest are so called active electronically scanned array (AESA) antennas, as seen in Figure 1.2. These are made up of a number of antenna elements put in a specific pattern. By phase shifting the signals transmitted by the antenna elements, it is possible to steer the main lobe of the antenna in different directions [7, p.1-59]. Because of this, the need of the antenna to rotate is eliminated. One disadvantage of using many different antenna elements is that they couple to each other, causing reflections at every port. This phenomena is dependent of the steering angle of the antenna. A consequence of this is that operating conditions of the elements in an AESA differ between its various ports when the steering angle is adjusted, which might change the amplitude of the outgoing signal from each of the antenna elements. It has been shown that such a variation in amplitude clearly worsen the performance of an AESA antenna [7, p.353-377]. One way to solve this problem could be to tune the output power of the amplifying element of each channel, resulting in a homogeneous output.

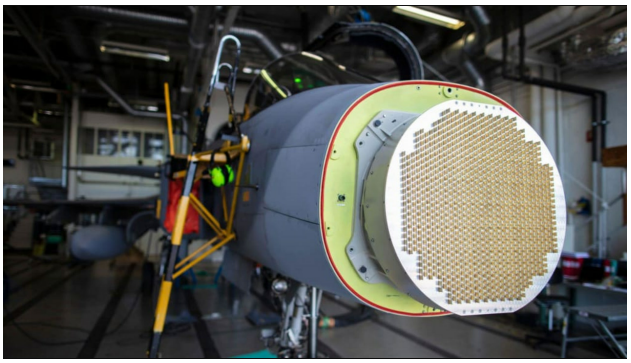

Figure 1.2: An AESA used in Saab's Gripen E, where each of the golden dots is one antenna element [1].

1.2 Aim

This master thesis will focus on the characteristics of load modulation and changing the point of operation that has been shown in the LMBA amplifier. More specifically it will be assessed if this can compensate for a bad output match or coupling which causes reflections, or bring advantages when operating in saturation in contrast to the shown advantages at back-off. Another factor to be assessed is whether there is a specific version of the LMBA [5] which is more favourable for this implementation. The purpose of the thesis is to examine whether or not these characteristics then can be considered beneficial for the radar systems at Saab.

1.3 Limitations

In accordance with most radar systems, this work will focus on one of the frequency bands - more precisely the S-band which covers frequencies from 2-4 GHz. As the time frame of this thesis is highly limited, there will be focus on a fast order time of components and printed circuit boards (PCB:s) when choosing suppliers. This aspect might also impact the scope of this work. Hence, there might be a trade-off in performance of the circuits and the extent of the report. In order for the design and simulation to be as close to the end result as possible, certain components might be chosen depending on the availability of rigid models and S-parameters for the chosen design software.

1.4 Ethical-, Societal- and Environmental Considerations

One ethical question regarding this work is raised through the fact that Saab is an arms company. As such, Saab does not only manufacture radars, but also weapon systems such as military aircraft, weapons, submarines and much more [8]. Hence, while this work primarily focuses on amplifiers for radar systems, it might also aid more offensive systems within Saab's arsenal. In turn, this could mean that the work could contribute to systems being used in warfare. However, it should be noted that Saab's product are focused towards defensive systems. While these still could be used in an offensive regard, it is not their intended use or application. Whether or not countries should have military systems at times of peace is a complex topic [9]. Though it is obvious that in the event of an attack, a country has the right to defend itself in order to make its citizens feel safe.

As mentioned in the introduction, the PAE at back-off has been proved to be better when using LMBA techniques. If this work were to prove that the PAE is increased in saturation also, or find that some other aspect of load modulation which might prove useful, it could be greatly beneficial for society. According to [10], the information and communication technologies stand for approximately 10 % of the world's energy consumption. One big part of making this industry environmentally sustainable is to make sure that the energy production itself is sustainable. However, an equally big part is that the energy consumption of the systems themselves are lowered, which partly is ensured by higher PAE of their components. One might argue that the larger impact on sustainability would be achieved by focusing on systems which operate at back-off, as this is the primary operational mode which communication systems operate in. Though, as most radars and other systems operate in saturation, this contribution cannot be neglected. There is also an argument that advancement in one of these technologies might breed advancements within the other one as well. Considering the extend to which wireless systems are integrated into society today, one could also assume that advancements within this area also would greatly impact society. One example of the impact of communication systems is the implementation of 5G [11].

2

Theory

In this chapter, a general overview of the theory behind this project is presented. Firstly, the theory behind an AESA and its reflection coefficient is discussed. Then the theory for a balanced amplifier is derived. Lastly, this theory is further developed and compared for four different topologies of the LMBA.

2.1 AESA

An AESA is an antenna which consist of multiple antenna elements, which is seen to the left in Figure 2.1. It is shown how the input signal is split into the M different antenna elements. Then, a phase shift $\Phi_m(\theta, \psi)$ is added to the input in order to steer the angle of the transmitted signal in elevation (θ) and azimuth (ψ). In order to understand more of how an AESA operates, the picture to the right of Figure 2.1 is studied. Here, the antenna elements are represented as triangles, $\vec{r}_m$ is the distance from the origin to element m and $\hat{r}$ is the direction of the outgoing field. Following [12, Chapter 2] and [13], each antenna is assumed to be voltage-driven elements which generate a field E_0 expressed as

$$E_0(r, \theta, \varphi) = V_0 F(\theta, \varphi) \frac{e^{-jkR}}{R}. \tag{2.1}$$

In the equation above, R is the distance from the element to a certain point in space, V_0 is the terminal voltage, $F(\theta, \varphi)$ is the dominant polarization or the element pattern and k is the wave number. In order to sum up the fields, one can define r as the distance to the element at the origin from a point in the far field in the $\hat{r}$-direction. Also, d_m is defined as the distance between element m and the element at origin in the $\hat{r}$-direction. As such, d_m can be used in order to calculate the difference in phase between the outgoing fields of these two elements. This yields a total field of

$$E(r, \theta, \varphi) = F(\theta, \varphi) \sum_{m=1}^{M} V_m \frac{e^{-jk(r-d_m)}}{r} = F(\theta, \varphi) \frac{e^{-jkr}}{r} \sum_{m=1}^{M} V_m e^{jkd_m}. \tag{2.2}$$

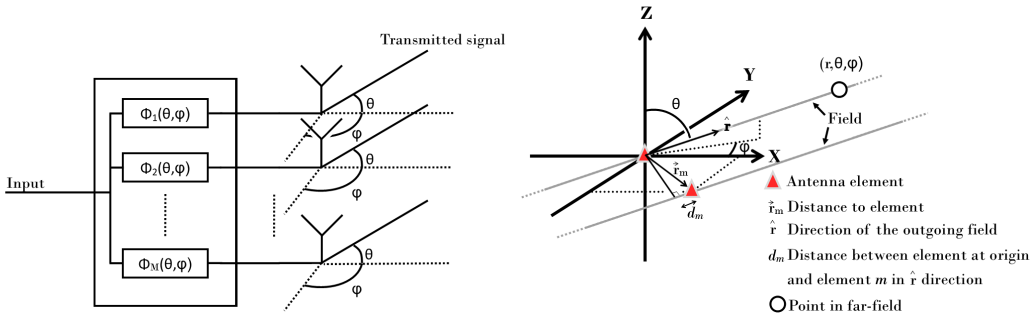

Figure 2.1: (Left) The basic structure of an AESA, where the signal for each antenna element is phase shifted individually before being transmitted. (Right) A representation of the antenna elements as triangles.

In order to calculate d_m, one can project $\vec{r}_m$ onto the unit vector $\hat{r}$. From the general spherical unit vectors, it is found that

$$\hat{r} = \hat{x}\sin\theta\cos\varphi + \hat{y}\sin\theta\sin\varphi + \hat{z}\cos\theta. \tag{2.3}$$

If all elements are assumed to be in the xy-plane, then

$$\vec{r}_m = \hat{x}x_m + \hat{y}y_m, \tag{2.4}$$

which yields

$$d_m = \frac{\vec{r}_m \cdot \hat{r}}{||\hat{r}||} = \sin\theta\cos\varphi x_m + \sin\theta\sin\varphi y_m. \tag{2.5}$$

Inserting this into equation (2.2) results in

$$E(r,\theta,\varphi) = F(\theta,\varphi)\sum_{m=1}^{M} V_m \frac{e^{-jk(r-d_m)}}{r} = F(\theta,\varphi)\frac{e^{-jkr}}{r}\sum_{m=1}^{M} V_m e^{jk(\sin\theta\cos\varphi x_m + \sin\theta\sin\varphi y_m)}. \tag{2.6}$$

The above equation expresses that when $\theta = 0$ and $\varphi = \pi/2$, the total field is at its maximum. In order to change this, and steer the output toward another angle θ_0, φ_0, the terminal voltage for element m is phase shifted as

$$V_m = v_m e^{-jk(\sin\theta_0\cos\varphi_0 x_m + \sin\theta_0\sin\varphi_0 y_m)}, \tag{2.7}$$

where v_m is the amplitude for element m. In turn, this changes equation (2.6) to

$$E(r,\theta,\varphi) = v_m F(\theta,\varphi)\frac{e^{-jkr}}{r}\sum_{m=1}^{M} V_m e^{jk[(\sin\theta\cos\varphi - \sin\theta_0\cos\varphi_0)x_m + (\sin\theta\sin\varphi - \sin\theta_0\sin\varphi_0)y_m]}. \tag{2.8}$$

Following the aforementioned argument, the field is now at its maximum at $\theta = \theta_0$ and $\varphi = \varphi_0$. However, changing the terminal voltage effects more than just the steering angle. To understand this, Figure 2.2 is examined, where an AESA is represented with voltage driven elements with impedances Z_0. Here, V_m^+ and V_m^- represent the incident and reflected voltages of element m. It is known that transmitting antenna elements that are placed close to one another will couple to each other, meaning that [13, 14]

$$V_m^- = \sum_{n=1}^{N} S_{mn} V_n^+, \tag{2.9}$$

where

$$S_{mn} := \frac{V_m^-}{V_n^+}\Big|_{V_k^+ = 0 \text{ for } k \neq n} \tag{2.10}$$

is called the Scattering parameters (S-parameters). Hence, for strong interference, equation (2.8) should be complemented with the above expression. Now, since the reflection coefficient Γ_m can be defined as

$$\Gamma_m = \frac{V_m^-}{V_m^+}, \tag{2.11}$$

equations (2.7) and (2.9) says that Γ_m will be dependent on the steering angles. More specifically,

$$\begin{aligned}\Gamma_m(\theta,\varphi) &= \frac{\sum_{n=1}^{N} S_{mn}V_n^+}{V_m^+} = \frac{\sum_{n=1}^{N} S_{mn}e^{-jk(\sin\theta_0\cos\varphi_0 x_n + \sin\theta_0\sin\varphi_0 y_n)}}{e^{-jk(\sin\theta_0\cos\varphi_0 x_m + \sin\theta_0\sin\varphi_0 y_m)}} \\ &= \sum_{n=1}^{N} S_{mn} e^{-jk[\sin\theta_0\cos\varphi_0(x_n - x_m) + \sin\theta_0\sin\varphi_0(y_n - y_m)]}.\end{aligned} \tag{2.12}$$

Equation (2.12) clearly states the the reflection coefficient is dependant on the steering angle of the AESA. Another way to interpret this is that the impedance of the antenna (Z_L) changes as the steering angle changes. This follows from the relation between reflection coefficient and the load impedance,

$$\Gamma = \frac{Z_L - Z_0}{Z_L + Z_0} \implies Z_L = Z_0\frac{1+\Gamma}{1-\Gamma}, \tag{2.13}$$

where it follows that any dependency in Γ will be dependencies of Z_L and vice versa.

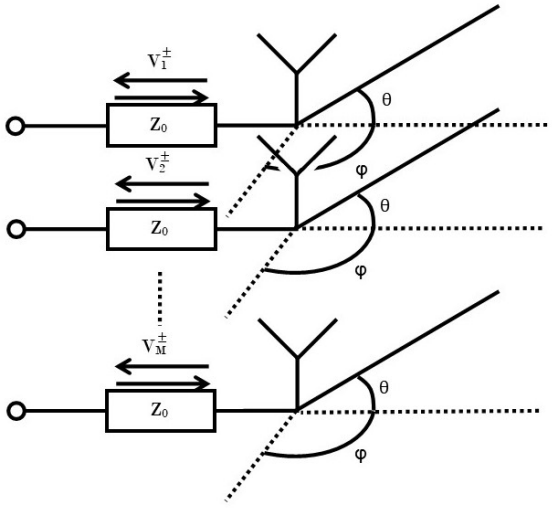

Figure 2.2: An AESA represented with voltage driven elements that has an impedance of Z_0.

2.2 Balanced Amplifiers

One question that is raised following the arguments in the previous section is how a difference in load impedance will effect an AESA's performance. Many systems implement a circulator or isolator in order to separate transmit- and receive modules as well as to get rid of unwanted reflections or coupling [12, Chapter 4]. However, these elements are known to be bulky, lossy and impractical to integrate [14, 15]. If there would be no way of separating the reflection from the channel, the change of load impedance would change the point of operation of the device closest to the antenna. For example, a different load impedance could change the characteristics of an amplifier, resulting in a change in output power or PAE. This can be further understood from the method of load-pulling amplifiers [16, Chapter 1]. This method is used in order to optimize one or more merit of performance of an amplifier by monitoring its characteristics while changing its load. Figure 2.3 shows how a Smith chart can look like during load-pull measurements, where the blue line represents values of PAE and the red lines represents output power. Smaller circles represents a higher value, and from the figure it is clear that it is difficult to optimize both parameters at the same time and that a small difference in the load might significantly impact the performance of the amplifier.

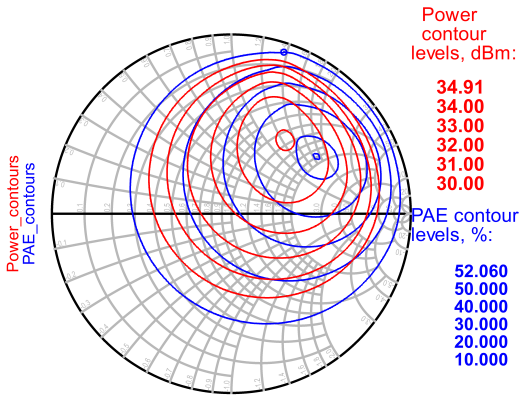

Figure 2.3: A general output of a load-pull measurement, where the load of an amplifier has been swept. The blue contours represent different values of PAE and the red ones different values of output power. Smaller circles equals higher values.

Another unwanted effect of a varying load impedance is that the reflection that arises might start to oscillate, causing instability in the system. As aforementioned, this might be solved by a circulator or isolator. However, given the drawbacks of such a component, an alternative might be to instead use a BA as a last device in the transmitting system. The basic topology of a BA can be seen in Figure 2.4 and consists of two identical amplifying elements which are put in parallel between two 90° hybrids.

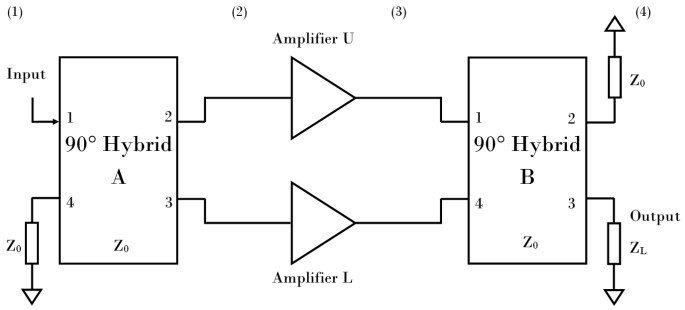

Figure 2.4: A general topology of a balanced amplifier, where two identical amplifying elements are put in parallel between two 90° hybrids.

In order to understand the operations of a BA, the characteristics of a 90° hybrid is examined. An ideal 90° hybrid should split its power between two ports, the coupled- and through ports. The signal at the coupled port will be shifted 90° in phase. The fourth port should be isolated with the same impedance as the hybrid [3, Chapter 7.5]. Hence, an ideal 90° hybrid has an S-matrix representation of

$$[S_{Hybrid}] = \begin{bmatrix} 0 & \frac{1}{\sqrt{2}} & j\frac{1}{\sqrt{2}} & 0 \\ \frac{1}{\sqrt{2}} & 0 & 0 & j\frac{1}{\sqrt{2}} \\ j\frac{1}{\sqrt{2}} & 0 & 0 & \frac{1}{\sqrt{2}} \\ 0 & j\frac{1}{\sqrt{2}} & \frac{1}{\sqrt{2}} & 0 \end{bmatrix}, \tag{2.14}$$

where the definition of S-parameters from equation (2.10) is used. Now, if the inputs of the system were to be represented by

$$[V_1] = \begin{bmatrix} V_{in} \\ 0 \\ 0 \\ 0 \end{bmatrix} \tag{2.15}$$

then V_1 passes through the first hybrid as

$$[V_2] = [S_{Hybrid}][V_1] = \begin{bmatrix} 0 \\ V_{in}/\sqrt{2} \\ jV_{in}/\sqrt{2} \\ 0 \end{bmatrix}. \tag{2.16}$$

If the amplifiers are presumed to be ideally matched with an amplification α, then

$$[V_3] = [\alpha][V_2] = \begin{bmatrix} \alpha V_{in}/\sqrt{2} \\ 0 \\ 0 \\ j\alpha V_{in}/\sqrt{2} \end{bmatrix}. \tag{2.17}$$

Lastly, the signal passes through the last hybrid which results in

$$[V_4] = [S_{Hybrid}][V_3] = \begin{bmatrix} 0 \\ \alpha\left(V_{in}/2 - V_{in}/2\right) \\ j\alpha\left(V_{in}/2 + V_{in}/2\right) \\ 0 \end{bmatrix} = \begin{bmatrix} 0 \\ 0 \\ j\alpha V_{in} \\ 0 \end{bmatrix} \tag{2.18}$$

As shown, the whole signal is recovered at the system's output port.

Moving on, if a reflected wave V_{ref} is travelling into port 3 of the second hybrid in Figure 2.4 and the output of the amplifiers are set to zero, the hybrid's output is

$$[V_{out,1}] = [S_{Hybrid}] \begin{bmatrix} 0 \\ 0 \\ V_{ref} \\ 0 \end{bmatrix} = \begin{bmatrix} jV_{ref}/\sqrt{2} \\ 0 \\ 0 \\ V_{ref}/\sqrt{2} \end{bmatrix}. \tag{2.19}$$

At the output of the amplifying elements, the signal will be reflected back towards the hybrid. Since the amplifying elements are identical, $\Gamma^U = \Gamma^L = \Gamma^{amp}$, the output will be

$$[V_{out,2}] = \Gamma^{amp}[S_{Hybrid}] \begin{bmatrix} jV_{ref}/\sqrt{2} \\ 0 \\ 0 \\ V_{ref}/\sqrt{2} \end{bmatrix} = \Gamma^{amp} \begin{bmatrix} 0 \\ jV_{ref} \\ V_{ref}/2 - V_{ref}/2 \\ 0 \end{bmatrix} = \Gamma^{amp} \begin{bmatrix} 0 \\ jV_{ref} \\ 0 \\ 0 \end{bmatrix}. \tag{2.20}$$

However, since port 2 of the second hybrid is isolated, this signal will dissipated by the impedance at this port. In other words, the reflection will not affect the rest of the system. The same argument as used above can also be used at the input of the amplifier to show that any mismatch at the input of the amplifying element will be dissipated at the isolated port of the first hybrid. It also shows that a signal in at the second port of the second hybrid will be retrieved at the output of the system.

In order to understand how a mismatched load might impact this system, the second hybrid of the BA is further examined. This can be seen in Figure 2.5. The goal of the analysis is to find the S-parameters of the system in order to retrieve the reflection coefficient at each of the ports. Since the ports are connected to the output of the amplifiers in the BA, this can be used to calculate the load that the amplifiers experience. The steps of the analysis are:

1. When calculating for port n, terminate all other ports with the characteristic impedance Z_0.
2. Excite port n with a voltage V.
3. Using the S-matrix for a hybrid in equation (2.14), calculate the reflected signals for each port.
4. Define the S-parameters using equation (2.10).
5. Repeat for all ports.
6. Excite all ports by using matrix multiplication, $[V^-] = [S][V^+]$, where the signal of the second port is 90° phase shifted from the one at the first port.
7. Find the reflection coefficient by the definition in equation (2.11).
8. By using the relation between reflection coefficients and impedances found in equation (2.13), express the impedance experienced by the respective amplifier.

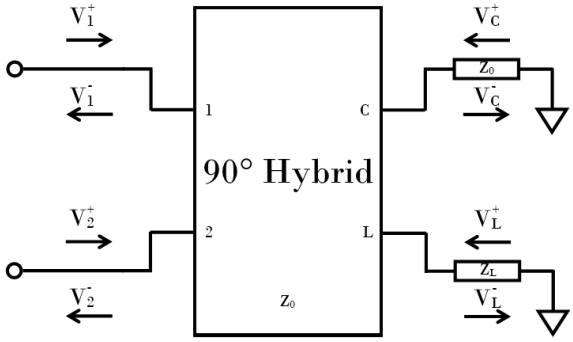

Figure 2.5: The image of the second hybrid in a balanced amplifier that is used to find the S-parameters.

By following the steps above, the resulting S-matrix of Figure 2.5 is

$$[S] = \frac{\Gamma_L}{2}\begin{bmatrix} -1 & j \\ j & 1 \end{bmatrix}, \tag{2.21}$$

where Γ_L is the reflection coefficient for the load. As explained, all of the ports were then excited with $[V^+] = [V_s, jV_s]$, where V_s is an arbitrary input signal. Then, the reflection coefficient and impedances can be found as

$$\begin{aligned} \Gamma_1 &= -\Gamma_L \\ \Gamma_2 &= \Gamma_L \end{aligned} \quad \Longrightarrow \quad \begin{aligned} Z_1 &= Z_0\frac{1-\Gamma_L}{1+\Gamma_L} \\ Z_2 &= Z_0\frac{1+\Gamma_L}{1-\Gamma_L}. \end{aligned} \tag{2.22}$$

Hence, it can be seen that a mismatch at the output impedance will make the reflection coefficient for the amplifiers move along the same line through the centre of the Smith chart. However, they will move in different directions. This can be seen in Figure 2.6. By studying Figure 2.3 as well, it can be seen that a small mismatch might slightly enhance the performance of one of the amplifiers. Although, since the loads move in different direction, one of them will most likely obtain different characteristics than the other one.

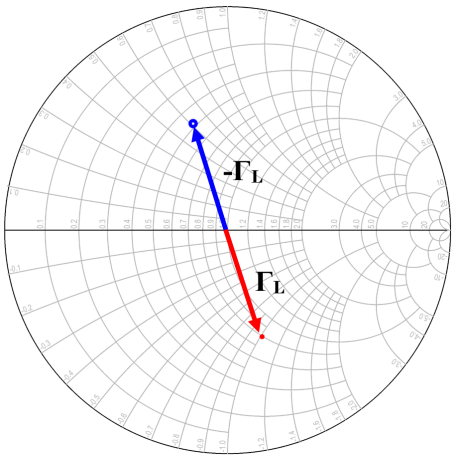

Figure 2.6: The loads that the upper (blue) and lower (red) amplifiers experience for a certain value of Γ_L. It is clear that they move in two different directions.

2.3 Load Modulation in Balanced Amplifiers

Instead of changing the point of operation of amplifiers by the mismatch of a load impedance, LMBAs feed the system with a control signal through the isolated output port of the second hybrid in a BA. There are a multitude of different ways of how exactly the control signal is fed into the system [5, 17, 18]. However, for the general analysis one can assume that it is fed from an external system with its own amplifier, as in Figure 2.7.

2.3.1 LMBA

As for the analysis of the BA, the second hybrid of an LMBA is analysed, which can be seen in Figure 2.7 [6]. It is assumed that the control signal is a factor β of the signal from the balanced amplifiers, meaning that $V_3 = \beta V_s e^{-j\phi}$. The variable ϕ is the phase of the signal in relation to the phase of V_s, which is controlled using a phase shifting element at this port.

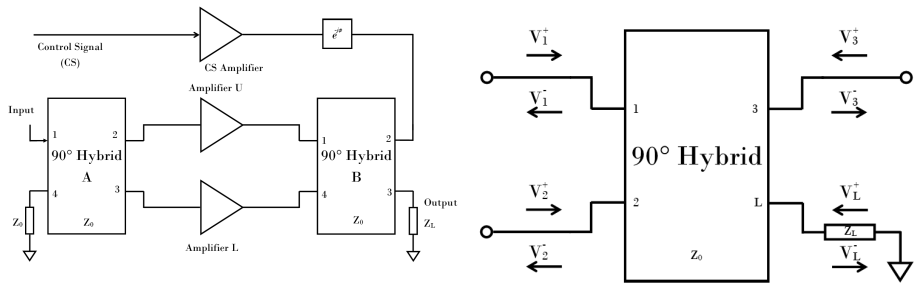

Figure 2.7: (Left) The basic structure for the LMBA, where the control signal is fed through a separate amplifier. (Right) The representation of the second hybrid in an LMBA that is used for analysis.

Once again the steps in section 2.2 is followed in order to yield the S-matrix for the system in Figure 2.7,

$$[S] = \begin{bmatrix} -\Gamma_L/2 & j\Gamma_L/2 & 1/\sqrt{2} \\ j\Gamma_L/2 & \Gamma_L/2 & j1/\sqrt{2} \\ j1/\sqrt{2} & j1/\sqrt{2} & 0 \end{bmatrix}. \tag{2.23}$$

When exciting all of the ports, the input signal is $[V^+] = [V_s, jV_s, \beta V_s e^{-j\phi}]$. As per previous arguments, the following reflection coefficients and impedances at the first and second ports are

$$\begin{aligned} \Gamma_1 &= -\Gamma_L + \frac{\beta e^{-j\phi}}{\sqrt{2}} \\ \Gamma_2 &= \Gamma_L + \frac{\beta e^{-j\phi}}{\sqrt{2}} \end{aligned} \quad \Longrightarrow \quad \begin{aligned} Z_1 &= Z_0 \frac{\sqrt{2} + \sqrt{2}\Gamma_L - \beta e^{-j\phi}}{\sqrt{2} - \sqrt{2}\Gamma_L + \beta e^{-j\phi}} \\ Z_2 &= Z_0 \frac{\sqrt{2} + \sqrt{2}\Gamma_L + \beta e^{-j\phi}}{\sqrt{2} - \sqrt{2}\Gamma_L - \beta e^{-j\phi}}. \end{aligned} \tag{2.24}$$

These results are fairly similar to the case of the BA. The reflection coefficients again move in separate directions, with the addition of the phase shifted term which are equal for the two ports. This means that the load which the amplifiers experience is tunable by changing β and ϕ. It should be noted that the only solution which yields $\Gamma_1 = \Gamma_2$ is for $\Gamma_L = 0$, meaning that the amplifiers never will experience the same load if the output is mismatched.

2.3.2 RLMBA

Using an external amplifier in order to feed the control signal into the system might not be desirable in all cases, for example if it would take up unwanted space. However, one might trade some degree of freedom in the load modulation in order to remove the need of this extra amplifier. In this report, three of these cases will be considered. The first one is the recursive LMBA (RLMBA) [17], where some of the output signal is coupled with a coupling of c to the control port in order to work as a

control signal. This can be seen to the left in Figure 2.8. As couplers generally have a fixed coupling

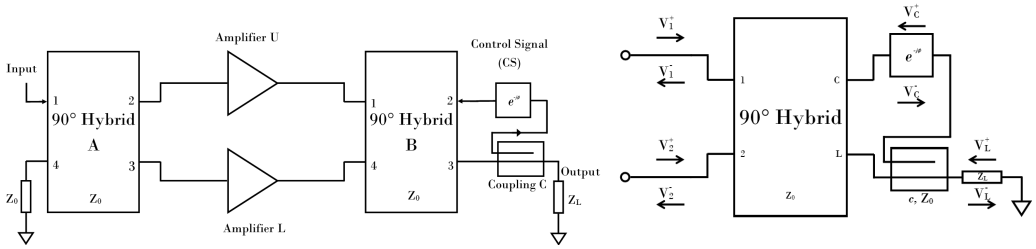

Figure 2.8: (Left) The RLMBA, where a part of the output signal is coupled to the control port in order to realize load modulation for the amplifiers. (Right) Representation used for calculations, in accordance with previous arguments.

factor c, this type of design can be assumed to have a fixed β in equation (2.24). This means that the load modulation is restricted to a circle, where the phase is decided by the phase shifter at the second port. In order to calculate S-parameters for the RLMBA, section 2.2 is followed resulting in

$$[S] = \begin{bmatrix} -\Gamma_L(1-c)^2/2 + jce^{-j\phi} & j\Gamma_L(1-c)^2/2 \\ j\Gamma_L(1-c)^2/2 & \Gamma_L(1-c)^2/2 + jce^{-j\phi} \end{bmatrix}. \tag{2.25}$$

In turn, this yields the reflection coefficients and impedances

$$\begin{aligned} \Gamma_1 &= -\Gamma_L(1-c)^2 + jce^{-j\phi} \\ \Gamma_2 &= \Gamma_L(1-c)^2 + jce^{-j\phi} \end{aligned} \implies \begin{aligned} Z_1 &= Z_0 \frac{1+\Gamma_L(1-c)^2 - jce^{-j\phi}}{1-\Gamma_L(1-c)^2 + jce^{-j\phi}} \\ Z_2 &= Z_0 \frac{1+\Gamma_L(1-c)^2 + jce^{-j\phi}}{1-\Gamma_L(1-c)^2 - jce^{-j\phi}} \end{aligned} \tag{2.26}$$

2.3.3 OLMBA

Another way to achieve LMBA behaviour without an external amplifier is by using the orthogonal LMBA (OLMBA) topology [18,19]. This can be seen to the left of Figure 2.9 and works by injecting the control signal into the isolated port of the first hybrid. This could be done through for example a splitter or a coupler, which eliminates the need for a third amplifier as the control signal will be amplified by the balanced amplifiers. Then the control signal is retrieved at the second port of the second amplifier, where it is met with a phase shifting element followed by an open circuit. As it will be reflected, it will then act as a control signal for the LMBA, as explained in section 2.3.1.

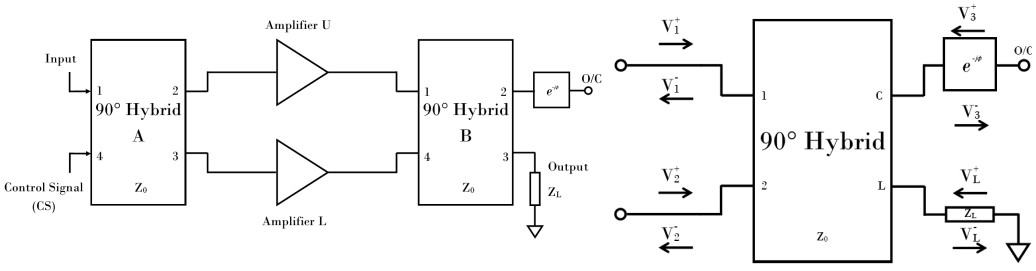

Figure 2.9: (Left) The OLMBA, where load modulation is achieved by inserting the control signal into the isolated port of the first hybrid. (Right) Representation used for calculations, as discussed in previous sections.

In the derivation of the reflection coefficients for this topology, it can be noted that the analysis will be the exact same as for the case with the LMBA. This is because the the whole control signal is retrieved at the third port of the hybrid, see the right of Figure 2.9. If β is used as the ratio between the control signal and the signal, then the only difference from the equations in the LMBA

case is that this time, the phase shift is 2ϕ instead of just ϕ, since the control signal passes through the phase shifting element twice. Hence, by using the same S-matrix and $[V^+]$ in equation (2.23), the reflection coefficient and impedance will be

$$\begin{aligned}\Gamma_1 &= -\Gamma_L + \frac{\beta e^{-j2\phi}}{\sqrt{2}} \\ \Gamma_2 &= \Gamma_L + \frac{\beta e^{-j2\phi}}{\sqrt{2}}\end{aligned} \quad \Longrightarrow \quad \begin{aligned}Z_1 &= Z_0 \frac{\sqrt{2} + \sqrt{2}\Gamma_L - \beta e^{-j2\phi}}{\sqrt{2} - \sqrt{2}\Gamma_L + \beta e^{-j2\phi}} \\ Z_2 &= Z_0 \frac{\sqrt{2} + \sqrt{2}\Gamma_L + \beta e^{-j2\phi}}{\sqrt{2} - \sqrt{2}\Gamma_L - \beta e^{-j2\phi}}\end{aligned} \tag{2.27}$$

2.3.4 RefLMBA

In the RLMBA and OLMBA topologies, there will always be load modulation present, even if the output would be matched. As is also the case with the LMBA, however in that case β can easily be set to zero by removing the drain bias of the control signal amplifier. One topology that only load modulates its amplifiers when the load is mismatched is one where the reflection itself is coupled to the isolated port of the second hybrid. Operating much like the RLMBA, this topology is named reflective LMBA (RefLMBA) in this paper and can be seen to the left of Figure 2.10. As for the

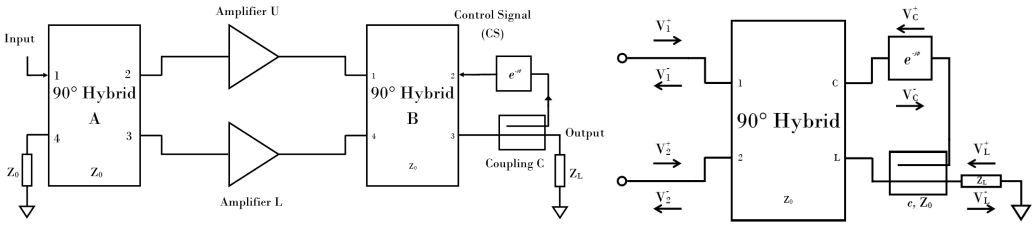

Figure 2.10: (Left) The RefLMBA, where load modulation is achieved by coupling the reflection to the isolated port of the second hybrid. (Right) Representation used for calculations, as discussed in previous sections.

previous topologies, section 2.2 is used to find the S-matrix of this topology. The result is

$$[S] = \frac{\Gamma_L}{2}\begin{bmatrix} c^2 e^{j2\phi} - (1-c)^2 + j2(1-c)c\,e^{j\phi} & jc^2 e^{j2\phi} + j(1-c)^2 \\ jc^2 e^{j2\phi} + j(1-c)^2 & -c^2 e^{j2\phi} + (1-c)^2 + j2(1-c)c\,e^{j\phi} \end{bmatrix}. \tag{2.28}$$

Per previous calculation, this yields

$$\begin{aligned}\Gamma_1 &= -\Gamma_L(1-c)^2 + j\Gamma_L(1-c)c\,e^{-j\phi} \\ \Gamma_2 &= \Gamma_L(1-c)^2 + j\Gamma_L(1-c)c\,e^{-j\phi}\end{aligned}$$

$$\Longrightarrow \quad \begin{aligned}Z_1 &= Z_0 \frac{1 - \Gamma_L(1-c)^2 + j\Gamma_L(1-c)c\,e^{-j\phi}}{1 + \Gamma_L(1-c)^2 - j\Gamma_L(1-c)c\,e^{-j\phi}} \\ Z_2 &= Z_0 \frac{1 + \Gamma_L(1-c)^2 + j\Gamma_L(1-c)c\,e^{-j\phi}}{1 - \Gamma_L(1-c)^2 - j\Gamma_L(1-c)c\,e^{-j\phi}}\end{aligned}. \tag{2.29}$$

As expected, the reflection coefficients equals zero when the output is matched ($\Gamma_L = 0$).

2.4 Comparison of Topologies

Below, a table with the different reflection coefficient for all of the topologies is presented. It is also stated what tunable parameters the system in question has. In the following subsections, the different reflection coefficients will be compared in Smith charts.

Table 2.1: The reflection coefficients for the discussed topologies.

Topology	**Reflection coefficients**	**Tunable parameters**
BA	$\pm\Gamma_L$	-
LMBA	$\pm\Gamma_L + \frac{\beta e^{-j\phi}}{\sqrt{2}}$	β, ϕ
RLMBA	$\pm\Gamma_L(1-c)^2 + jc\,e^{-j\phi}$	ϕ
OLMBA	$\pm\Gamma_L + \frac{\beta e^{-j2\phi}}{\sqrt{2}}$	ϕ
RefLMBA	$\pm\Gamma_L(1-c)^2 + j\Gamma_L(1-c)c\,e^{-j\phi}$	ϕ

2.4.1 Matched Case

Firstly, the Smith charts of the matched case for the different topologies are studied. This can be seen in Figure 2.11. Here, the phase of the control signal ϕ is swept from 0 to 2π, and β or c in Table 2.1 is 0, 0.1 and 0.5. This is to correspond to a fraction or coupling of $-\infty$, -10 or -3 dB. In order to understand the charts, it is beneficial to start by studying the BA, which operates without load modulation. Since it is matched, the respective reflection coefficient is at the middle of the Smith chart. In accordance with Table 2.1, the same holds for the RefLMBA. For the three other topologies, the control signal forms circles around the centre of the Smith chart. A larger β or c corresponds to a larger radius and tuning ϕ changes the phase of the reflection coefficient along this circle. Another noteworthy observation is that the reflection coefficient assumes the same values for both of the amplifiers.

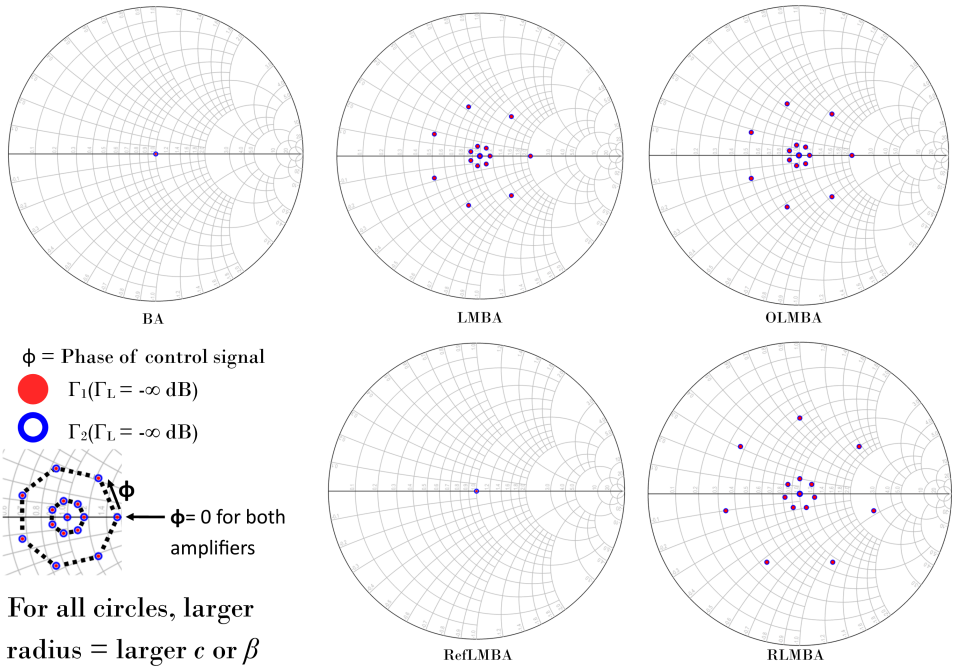

Figure 2.11: The reflection coefficients of Table 2.1 plotted in Smith charts for the matched case. The phase ϕ is swept from 0 to 2π and values of c or β are 0, 0.1 and 0.5.

2.4.2 Unmatched case

Since a lot of factors change for the unmatched case, it is explained using two pictures. Initially, the reflection coefficients are studied with a Γ_L of $-6\,\text{dB}$, but with an arbitrary phase (θ). This can be seen in Figure 2.12. The key takeaway from this case is that the reflection coefficients ends up at opposite sides of the Smith chart, but otherwise the patterns represents the same points. This means that the control signal still affects the reflection coefficients in the same way. One way to think of it is that first, the mismatch moves the reflection coefficients in opposite directions, which can be seen in the Smith chart for the BA in 2.12. Then, the amplitude of the control signal moves the reflection coefficients a certain length from the mismatch in the same direction for both of the amplifiers. Then, the phase of the control signal rotates the reflection coefficients in the same direction for both of the amplifiers. For example, the point furthest to the right for both reflection coefficients corresponds to the same mismatch of the system, amplitude of the control signal and phase of the control signal. This is illustrated to the bottom left of Figure 2.12.

As opposed to the matched case, it is clear that both the BA and RefLMBA are affected more for the mismatched case. This is expected from the derived equations. One can also note that the behaviour of the load modulation can be put into two categories. The LMBA and OLMBA both form circles around the mismatched reflection coefficients, which is seen if one compares these Smith charts with the one for the BA in Figure 2.12. The other category is the RefLMBA and RLMBA, which moves further towards the centre of the Smith chart for larger control signals.

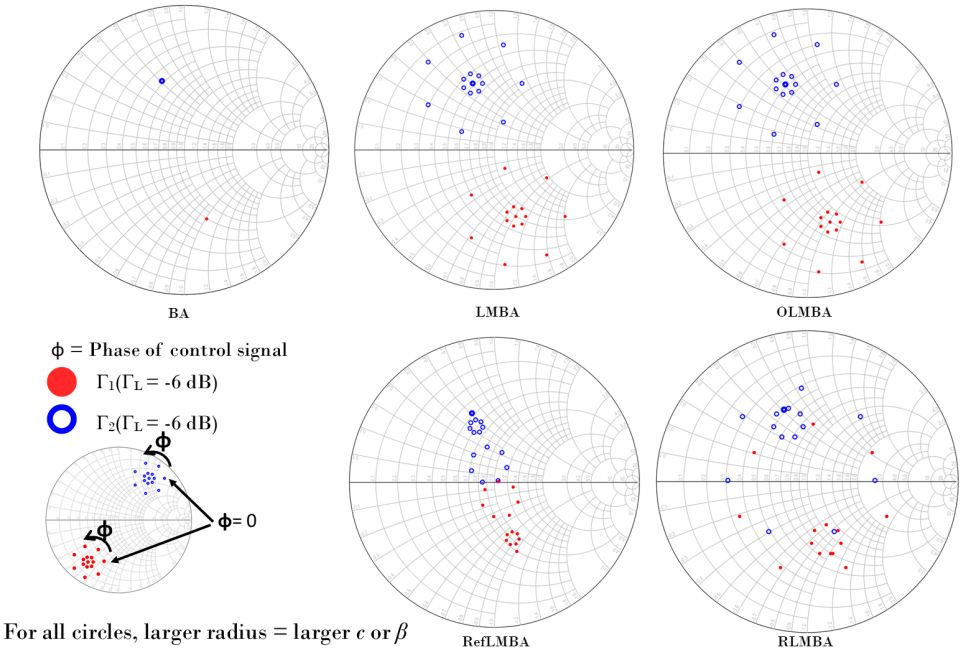

Figure 2.12: The reflection coefficients of Table 2.1 plotted in Smith charts for the unmatched case $\Gamma_L = -6\,\text{dB}$ with an arbitrary phase. The phase ϕ is swept from 0 to 2π and values of c or β are 0, 0.1 and 0.5.

Next, the aforementioned case is further developed as θ is swept from 0 to 0.9π. These plots can be seen in Figure 2.13, and if one compares these to Figure 2.12, it is clear that the phase of Γ_L rotates the reflections coefficients in the same direction around the centre of the Smith chart. This is why θ is not swept any further, as this would make it too cluttered and hard to see which reflection coefficient that corresponds to what values. As the Smith chart for the RLMBA topology still gets cluttered, there is a magnification of the pattern for one value of θ for clarity.

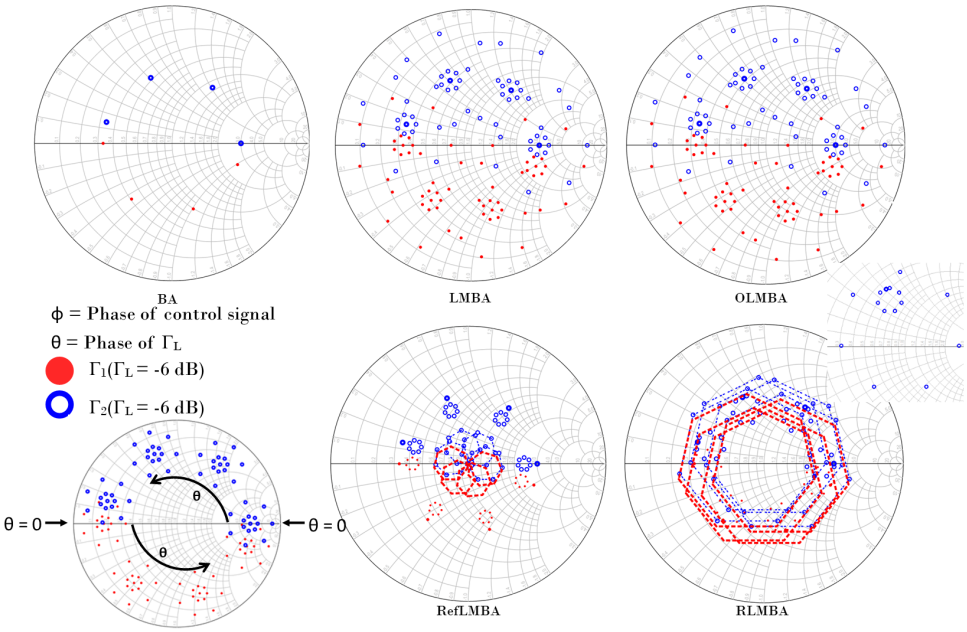

Figure 2.13: The reflection coefficients of Table 2.1 plotted in Smith charts for the unmatched case $\Gamma_L = -6\,\text{dB}$ with swept phase θ from 0 to 0.9π. The phase ϕ is swept from 0 to 2π and values of c or β are 0, 0.1 and 0.5.

In most systems, there is a clear advantage to not being forced to actively tune the phase of a signal. Also, the phase of Γ_L might shift rapidly or be completely random. Hence, it is of interest to see how the reflection coefficients behave when the θ is swept for constant values of ϕ. This case can be seen in Figure 2.14. Here, β and c are at a constant value of 0.5. Studying these plots proves that there might be an inherent advantage to using the RefLMBA or RLMBA, as these form circles closer to the centre of the Smith chart.

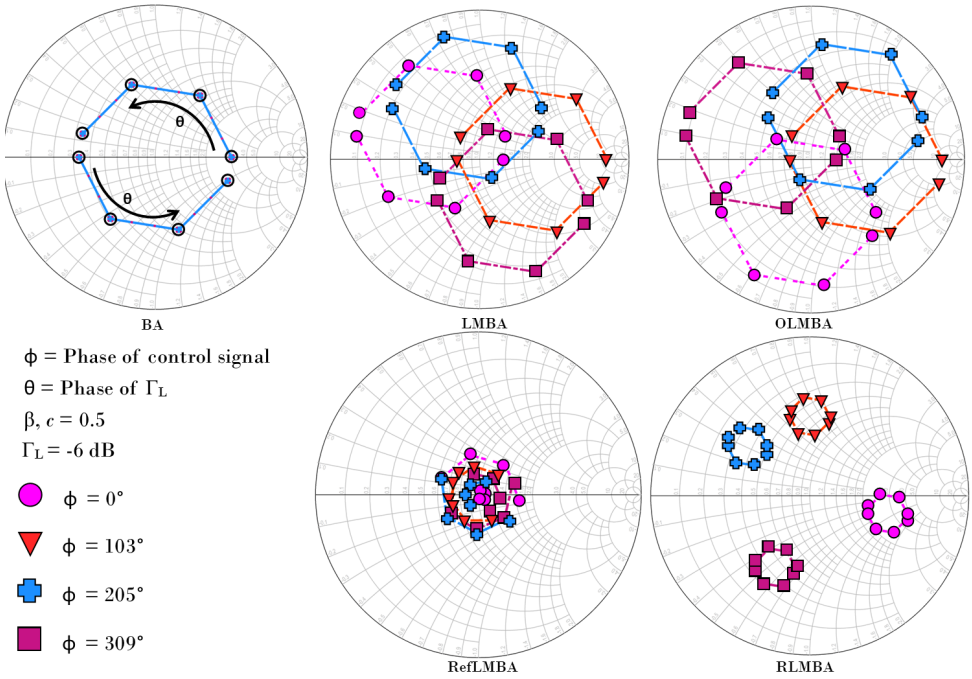

Figure 2.14: The reflection coefficients of Table 2.1 plotted in Smith charts for the unmatched case $\Gamma_L = -6\,\mathrm{dB}$ with swept phase θ from 0 to 0.9π. The phase ϕ is held at constant values between 0 and 2π. Also, c or β are set to 0.5.

3
Methods

In this chapter, the methods that were used during this thesis work are discussed. After the theoretical background in chapter 2, simulations using Keysight's Advanced Design Systems (ADS) were performed. Firstly, the working method of load modulation was proved for the matched case with ideal components, which one by one were switched out for non ideal ones. Then, the unmatched case was considered in order to try whether the derived theoretical equations were correct or not. As a last step, the load modulating technique was tested in a lab using test circuits and external components.

3.1 Simulation

The first step towards examining the behaviour of the various LMBA architectures was to try and achieve load modulation using simulation software. Hence, the initial step was a simulation using ideal components in ADS for a matched system. For this, the programme's 'Harmonic Balance' simulation was used. As load modulation was achieved, each ideal component was switched out with its non ideal counterpart. This was initially done with the amplifier, which had been built and characterised at Saab. Apart from being operational within S-band, notable characteristics of the amplifier was that it were output matched. Because of its in-house manufacturing there were rigorous models available for simulation. The biasing and input power needed for the amplifiers were also available. Although, the input power was examined by plotting the output power for various input power levels in order to verify that the amplifier was working in compression. Then, each of the couplers were replaced with S-parameter models of non ideal ones. These were chosen based on availability, both of actual components and rigid S-parameter models. The models for two couplers were used, a 3 dB coupler [20] and a 10 dB coupler [21], both from Anaren. This meant that the cases that were being examined was for a c or β of -10 dB and -3 dB. As the simulations grew more complex, the solver was switched out to 'Krylov' in order to make the simulations converge. As a last step, 50 Ω transmission lines were added between the components. Its characteristics were calculated using the programme's 'LineCalc' function, based on the same substrate that were used for the amplifier. The lengths were swept from 0 to $\lambda/2$ for 2 GHz, which is the lower bound for the S-band and hence has the longest wavelength. This was done in order to ensure that no instability was introduced for certain lengths. Though, the lengths for certain transmission lines were always put to be equal one another in order to achieve good, balanced behaviour. As a phase shifting element, a transmission line was used, where its length was swept in order to obtain different phase shifts.

During the simulations, the 'Gamma Probe' in ADS was used in order to verify the reflection coefficients for the amplifiers. As this figure of merit is not measured easily in a lab, PAE and output power were two figures of merit that also were examined in order to verify the characteristics in previous reports. A full view of the simulations for the RLMBA topology is seen in Figure 3.1. The same simulation settings were used for the other topologies, discussed in section 2.3.1. The only difference was for the LMBA topology where a coupler was used at the input of the system to decouple some of the input signal as the control signal. The reason why this topology was used was to eliminate external factors from another amplifier while comparing this topology to the others.

The different topologies were then simulated for the unmatched case. This raised a few problems,

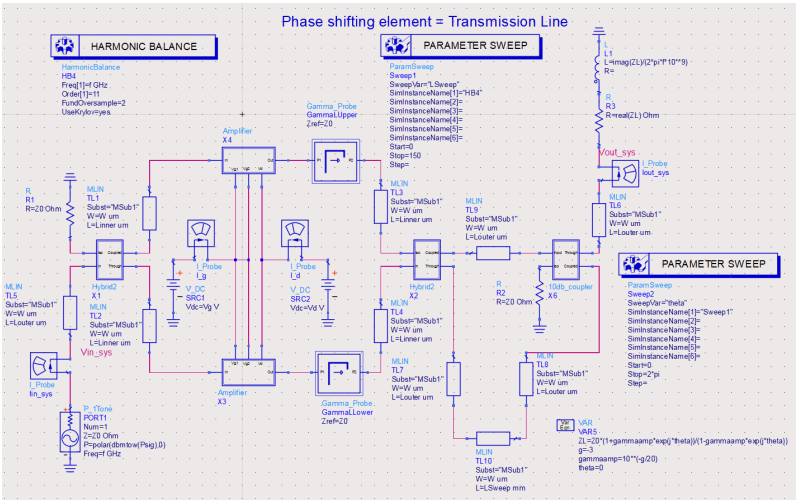

Figure 3.1: The setup that was used in ADS to verify the load modulation behaviour for the different topologies. Here, the setup for the RLMBA is pictured.

as the simulator had a hard time converging. In order to try and make it easier for the simulator to converge, multiple actions were taken. At first, the solver's 'Convergence mode', 'Max. Iterations' and 'Krylov Restart Length' were set to 'Robust'. Then, the 'Harmonic Balance Assisted Harmonic Balance' and 'Regenerate Initial Guess' were both activated. When some topologies still did not converge, the transmission lines were removed and the 'PhaseShifterSML'-component was added as a phase shifting element. As the simulations only considered a fixed frequency, this component was considered a sufficient replacement for the transmission line. However, the LMBA and OLMBA topologies still did not converge. The reason behind this was thought to be due to the fact that the reflection originating from the mismatch created oscillation in these topologies, but not in the RLMBA and RefLMBA ones as these used couplers which causes a loss for the reflections. As such, two attenuators were added, one by the load of the system and one at the isolated port of the second hybrid. The values of both of these was put to 1 dB, which could be viewed as losses between interfaces in a real system. After all of the topologies were able to converge, the real simulations were made. These were done by first sweeping ϕ from 0 to 2π and θ from 0 to 0.9π as well as setting Γ_L to -6 dB and $-\infty$ dB.

Another simulation that was done was to conduct a load-pull of the amplifier in question. By doing this, an approximation was given of how the performance of the amplifier was affected by a difference in its impedance. For the purpose of understanding how the load-pull is affected by different parameters, the load-pull was done while sweeping the frequency over a select part of the S-band and the input power from an arbitrary power level P_0 to P_0+30 dBm. This caused the amplifier to be swept from linear operation to operation in saturation.

3.2 Measurements

The purpose of the measurements was to prove the concept of load modulation. Because of this, already available printed circuit boards (PCB:s) and external components were considered sufficient. The measurement setup can be seen in Figure 3.2. Every instrument in the setup was controlled through MATLAB with general purpose interface bus (GPIB), and the full code can be found in Appendix A. The principle behind the measurement was that first, all of the instruments were set to their factory presets. Then, the preamplifier (Mini circuit's ZHL-5W-422X+) and the drain voltage of the amplifier was turned on through one power supply (Agilent's 6643A) each. After this a function generator (Tektronix' AFT31000) was turned on. This instrument had a twofold purpose as it both pulsed the gate of the amplifier with a bias and sent a trigger to the 'Pulse input' port of a vector network analyser (VNA, Keysight's ENA E5080B). This made the

VNA send an RF pulse to the amplifier. This pulse was designed to be shorter than the pulse that the function generator sent to the amplifier's gate, meaning that the RF signal was contained within the gate voltage's pulse. It was also important that the RF pulse started when the gate voltage had reached a stable level, which is why a delay was implemented between the trigger's arrival and the transmission of the pulse. This was because of the high power being sent into the amplifier, which might have turned on its transistors even though the gate voltage was turned of. The reason behind the pulsed measurements being used was because of the amplifiers' high operating power, which made this necessary to keep its temperature down.

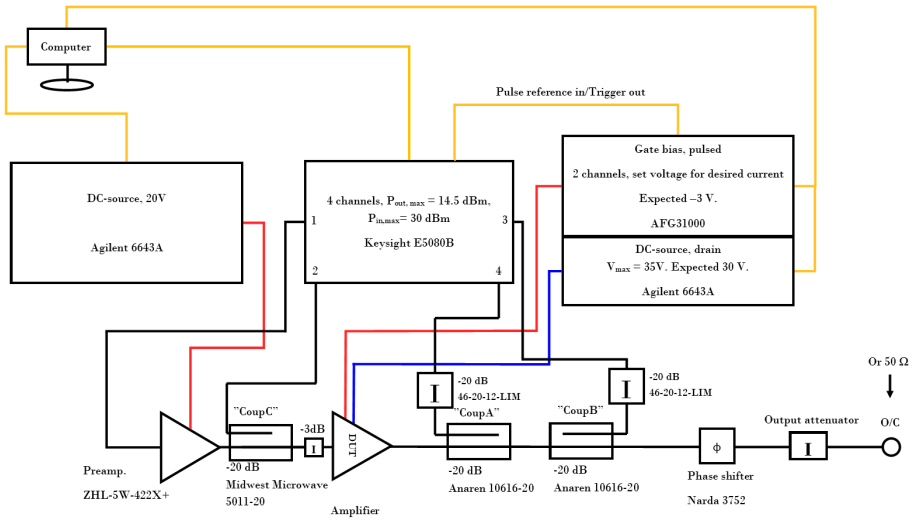

Figure 3.2: The measurement setup used for all of the measurements. This setup shows a single amplifier marked 'DUT', which is replaced for other topologies.

In Figure 3.2, there are also some extra couplers and attenuators. The 3 dB attenuator at the input of the amplifier was added to stop eventual oscillations from starting as a consequence of a mismatch in impedances between two amplifying elements. The two 20 dB attenuators (46-20-12-LIM) were put in place to protect the VNA in case of oscillation in the amplifiers, which would cause the amplifiers to output maximum power. The couplers were in place to monitor one figure of merit each. CoupC (Midwest Microwave 5011-20) monitored the power which was emitted out of the preamp, CoupA (Anaren 10616-20) monitored the output power of the amplifier and CoupB (Anaren 10616-20) monitored the reflection from the load. The latter was to be used for calculations of the reflection coefficient to make sure it had a value of -3 dB. In order to measure a matched case, the system was terminated with 50 Ω. When measuring a mismatched load, this was simulated by opening the circuit and placing an attenuator by the output. To sweep the phase of the reflection coefficient, a phase shifter (Narda 3752) was used. When measuring other topologies, the same setup was used but with another device under test (DUT). However, all setups had in common that they were balanced by using two 90° couplers (XC3500M-03S) found on another PCB. A complete collection of all of the DUT setups can be found in Appendix B.

The measurements that were done were two different sweeps, one for frequency and one for input power. These sweeps were firstly done for all of the components in the circuit separately to be able to subtract the S-parameters for these elements in order to retrieve the characteristics of the amplifier itself. When measuring on the amplifier, the primarily monitored figures of merit were the output power and PAE, where the input powers were monitored from the VNA and the power supplies. A complete list with all of the variables that were set during the measurements can be seen in Table 3.1.

Table 3.1: All of the variables that were set during the measurements for the two different sweeps.

Parameter	V_{preamp}	V_D	$V_{G,high}$	$V_{G,low}$	Duty	Period
For all sweeps	28 V	30 V	Search for I_D =1.1 A	−5.5 V	10 %	100 µs

Parameter	P_{start}	P_{stop}	f_{start}	f_{stop}
Power sweep	−30 dBm	10 dBm	3 GHz	-
Frequency sweep	Search for 21 dBm into amplifier	-	10 MHz	6 GHz

4

Results

In this chapter, the results are presented and discussed. Firstly, the simulated reflection coefficients and load pull measurements are shown in Smith charts, followed by some figures of merit retrieved from the measurements.

4.1 Smith charts

Following section 2.4, Smith charts following the simulations are presented below. Starting with the matched case of the amplifiers, the figure below should be examined while considering Figure 2.11.

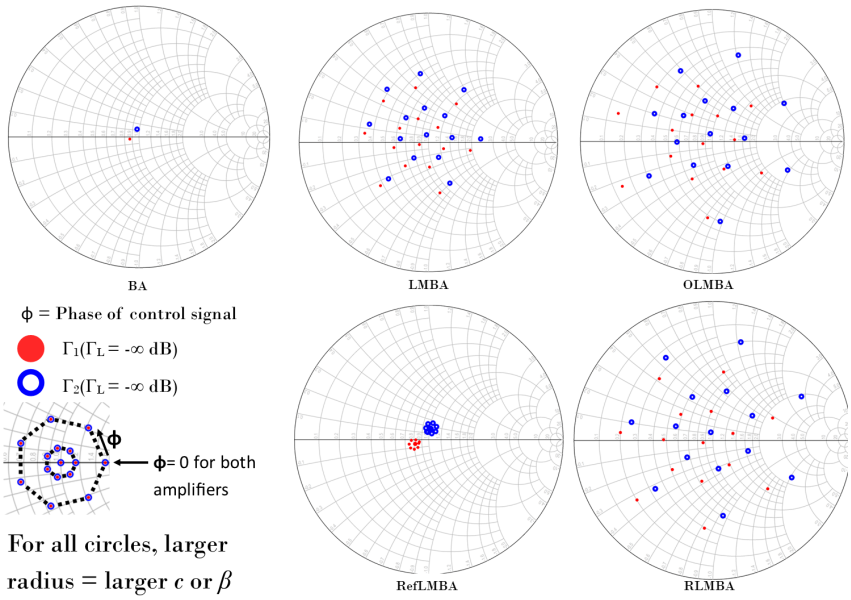

Figure 4.1: The simulated reflection coefficients plotted in Smith charts for the matched case. The phase ϕ is swept from 0 to 2π and values of c or β are 0, 0.1 and 0.5.

Next, the mismatched case with a Γ_L of -6 dB and arbitrary phase is considered This is considered in regard to Figure 2.12.

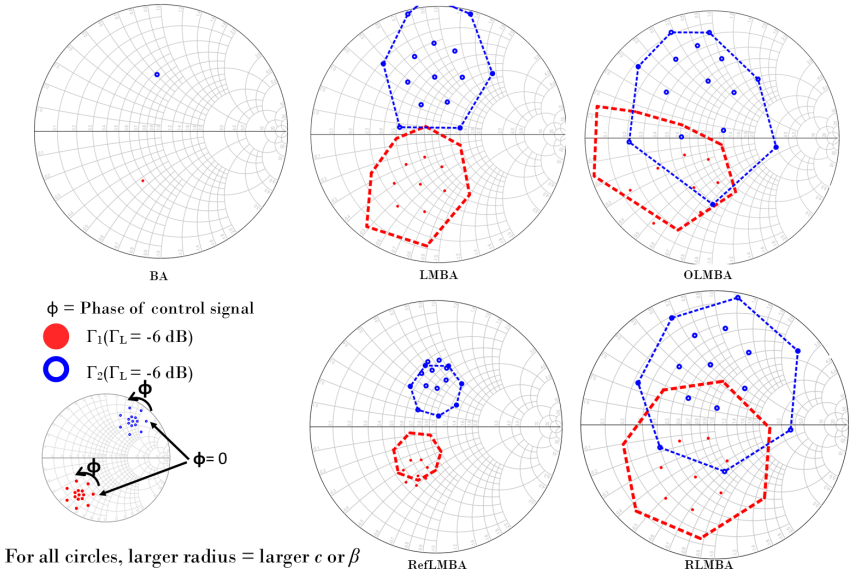

Figure 4.2: The simulated reflection coefficients plotted in Smith charts for the unmatched case with a Γ_L of -6 dB and arbitrary phase. The phase ϕ is swept from 0 to 2π and values of c or β are 0, 0.1 and 0.5.

Moving on, the aforementioned case is presented for a swept θ from 0 to 2π. As in its equivalence in Figure 2.13, some of the plots becomes very cluttered. Hence, it is recommended to study this and Figure 4.2 at the same time.

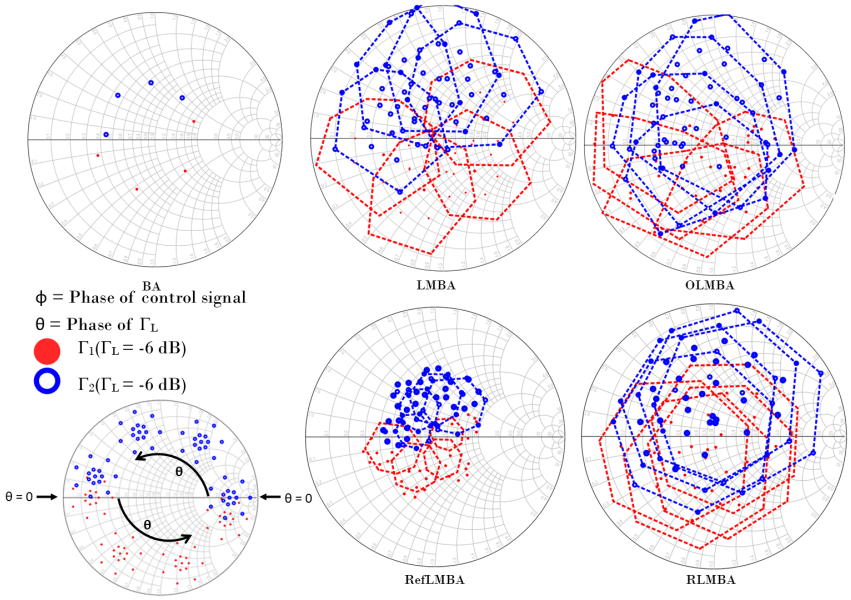

Figure 4.3: The simulated reflection coefficients plotted in Smith charts for the unmatched case with a Γ_L of -6 dB and a swept θ from 0 to 2π. The phase ϕ is swept from 0 to 2π and values of c or β are 0, 0.1 and 0.5.

Lastly, the results in Figure 4.3 are presented for different constant values of ϕ and a constant value of β or c as 0.5. This can be compared to Figure 2.14

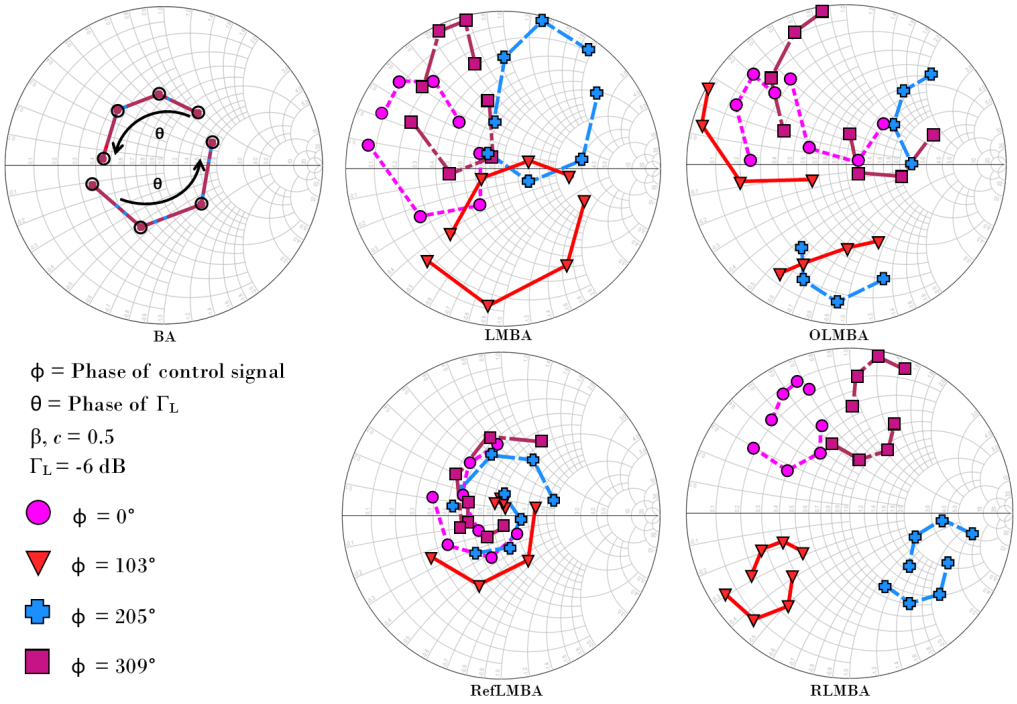

Figure 4.4: The simulated reflection coefficients plotted in Smith charts for the unmatched case with a Γ_L of -6 dB and a swept θ from 0 to 2π. The phase ϕ is set to some constant values and c or β are 0.5.

By comparing the Smith charts for the reflection coefficients in this section and section 2.4, one can tell that the derived theory somewhat concurs with the simulated results and that in this system, the amplifiers are not perfectly matched. Notable differences are that the simulations produce more of an elliptical shape in contrast to the perfect circles of the theory and that the reflection coefficient are not perfectly centred around the matched case for the LMBA and OLMBA. One obvious explanation to the differences is the fact that the theoretical system was considered without imperfections. One could derive the extent of the effects of the imperfections introduced when using non ideal components. However, the purpose of the theoretical equations are to get an idea of how the reflection coefficients act in the different topologies. As imperfections of the hybrids, the matching of the amplifiers, the lengths of the adjoining conductors and much more affects the reflection coefficient, rigorous simulations should be considered a better tool to calculate these.

Another conclusion that can be drawn from the Smith charts are that the RefLMBA in general should be closer to the matched case than the other topologies when a large coupling of the reflection is used. It also has the inherent advantage of being perfectly matched when there is no mismatch. Although, when a higher coupling is used at the output of the RefLMBA, there will be a higher loss of power. This system could also be more prone to starting to oscillate. The loss of power is something that is not as prominent in the RLMBA, as it couples some of the output signal as its control signal. However, in this case the power loss is represented by how much of the reflected signal that is coupled to the isolated port of the coupler. In the case of the LMBA and the OLMBA, losses will not be as much of an concern. Instead, the lack of losses might create oscillations if the mismatch is too great, as could be seen when trying to simulate these circuits in section 3.1.

4.2 Load Pull

In this section, the result of the load pull simulations of a single amplifier are presented. First, to the left in Figure 4.5, the power is swept during the simulation. Crosses represents the load yielding the maximum PAE and circles the load corresponding to the maximum output power (Pout). It can be seen that these points does not move too far while sweeping the input power. Secondly, to the right of Figure 4.5, the frequency is swept during the load pull. The symbols represents the same figures of merit as for the previous figure, and it is clear that now, the maxima moves much more.

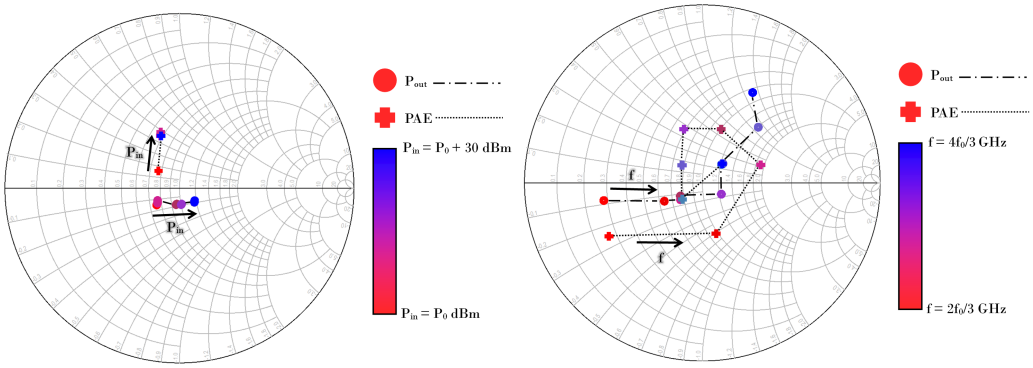

Figure 4.5: (Left) The simulated load pull measurement while sweeping the input power, where each point represent the load yielding the maxima for the respective figures of merit. (Right) The simulated load pull measurement while sweeping the frequency, where each point represent the load yielding the maxima for the respective figures of merit.

Studying the Smith charts during the load pull simulations, one might assume that these amplifiers were designed with a priority of high output power instead of PAE. It is also clearly shown that while both output power and PAE are dependent of the input power, it is much more dependent upon frequency. As this load pull was done for a single amplifier and not the BA, the bandwidth of the hybrids used should be taken into consideration when discussing the BA.

4.3 Measurements

Here, the results from the measurements are presented. In the measurements, the amplitude of Γ_L were constantly $-3\,\text{dB}$ while ϕ and θ were swept for each topology. Initially, the overall performance of each topology with regard to output power is presented in Figure 4.6. The output power is normalized to the output power of the matched BA, and for each θ the maximum and minimum value for each ϕ is presented. Hence, this can be seen as the range of the output power which is available for each ϕ when θ is unknown. Furthermore, the same plot but for PAE is presented in Figure 4.7. Note that in both of these plots, each symbol represents the same ϕ.

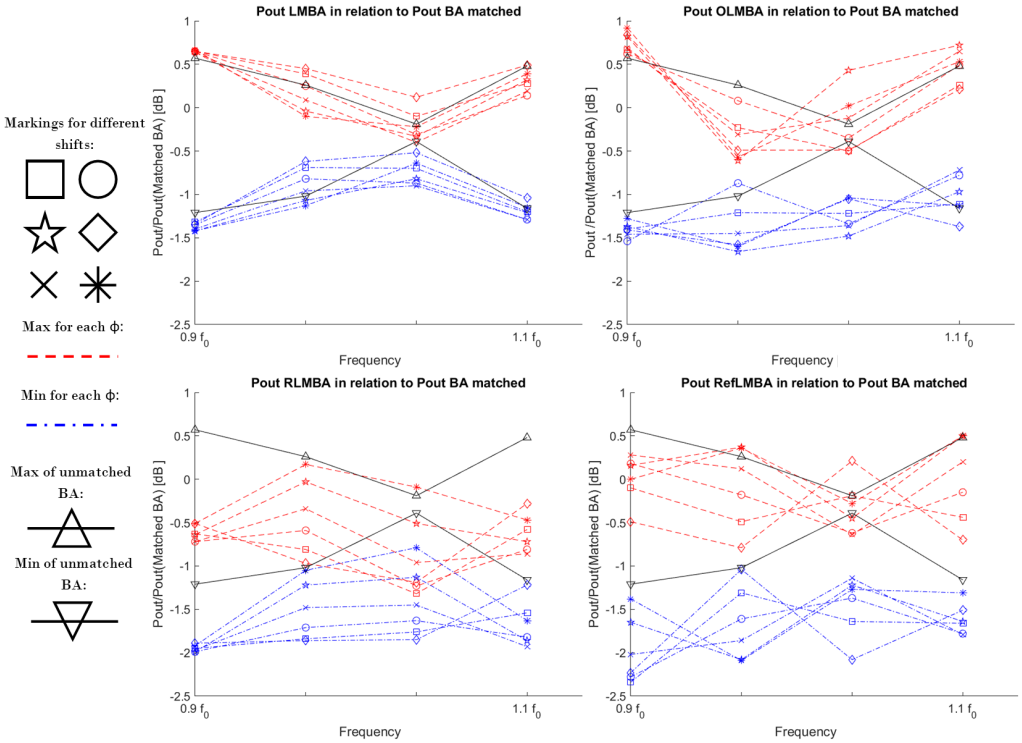

Figure 4.6: Output power of the amplifier in the different topologies, normalized to the output power of the BA. Each line represent the maximum or minimum output power for a certain ϕ when sweeping θ.

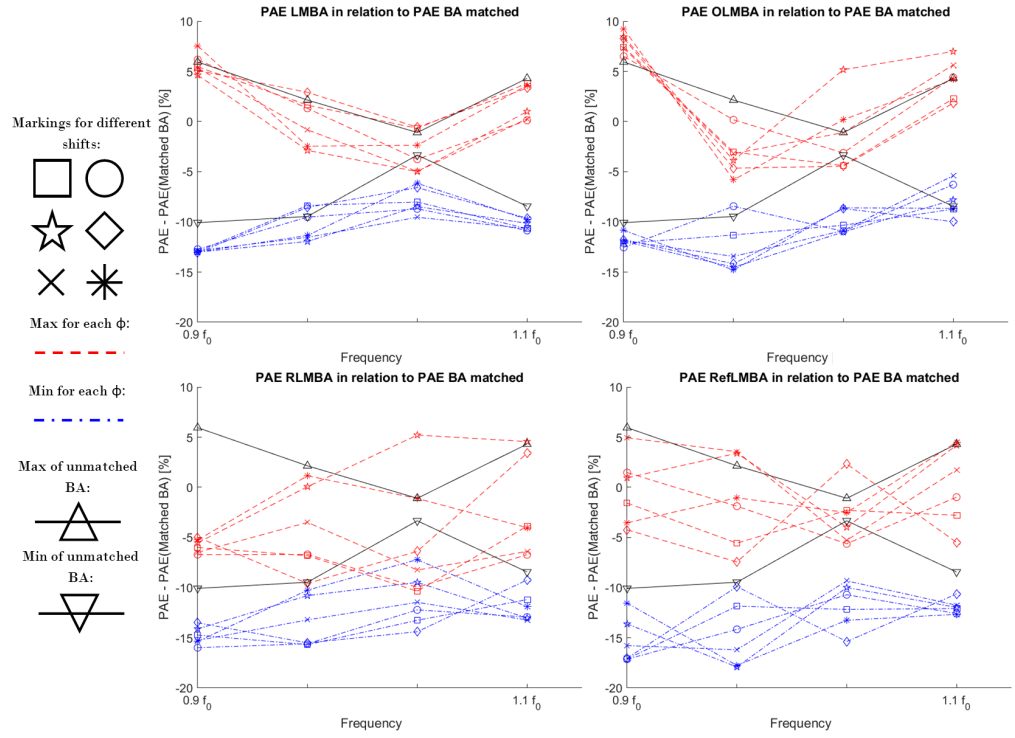

Figure 4.7: PAE of the amplifier in the different topologies, normalized to the output power of the BA. Each line represent the maximum or minimum output power for a certain ϕ when sweeping θ.

Moreover, to the left of Figure 4.8, the maximum output power for all of the mismatched topologies are presented as normalized to the output power of the matched BA. To the right of Figure 4.8, the same plot is presented but for PAE.

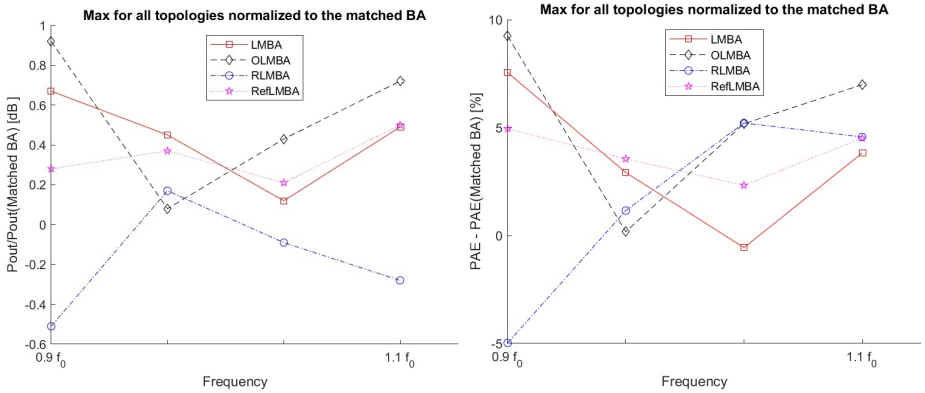

Figure 4.8: (Left) Maximum output power for the different mismatched topologies normalized to the output power of the matched BA. (RIGHT) Maximum PAE for the different mismatched topologies normalized to the output power of the matched BA.

The purpose of presenting the measurements as it is done in Figure 4.6 and 4.7 is twofold. Firstly, it is used to point out that when using load modulation in this manner, one particular phase shift of the control signal is not guaranteed to always produce a good operational point for the amplifier. For this purpose, it is beneficial to study Figure 4.4 as well. The plots in Figure 4.6 and 4.7 represents the best and the worst points of operation for each line in Figure 4.4. However, it should be noted that in the measurements another value of β and c were used, meaning that the actual reflection coefficients looks a bit different. Using this argument, one could assume that the shifts in Figure 4.6 and 4.7 that has lower spread are due to the fact that this shift forms a smaller circle somewhere on the Smith chart. On the other hand, the lines with a large spread can be seen as having one point of mismatch which brings them close to the centre of the Smith chart while another point brings them further from the centre. This is illustrated in Figure 4.9.

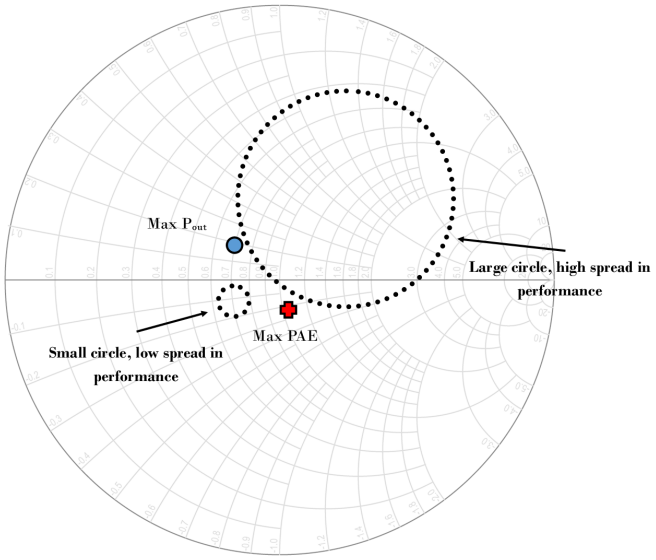

Figure 4.9: Illustration of how different characteristics of the topologies' reflection coefficient might impact its spread in performance.

The other purpose of these plots is to show that the amplifiers have different operating points which yield higher output power or better PAE, see the load pull in Figure 4.5 or the illustration in Figure 4.9. This does not mean that a point which yields high output power cannot yield better PAE, but it should not be a precise correlation between these to figures of merit. However, as these amplifiers are well matched to begin with, many of the good operating points are the same. Though, as the plots are showing, there is not a complete correlation between good or bad output power and PAE.

Next, the plots in Figure 4.8 is considered. In these, the maximum performance for each of the topologies are presented. In contrast to Figure 4.7, this represents choosing the phase shift of the control signal which always yields the best performance. Here, it is also clear that there is not a perfect correlation between highest output power and best PAE. However, it is clear that while actively tuning the control signal, it is almost always possible to slightly enhance the performance of the amplifier. It is interesting to note that the increase in performance is generally higher at the edges of the measured frequency range. This is thought to be because these points lay outside of the bandwidth of the amplifier. Circling back to the simulated load pull of Figure 4.5, it becomes intuitive to think of this as re-matching the amplifier to these points. It might also explain why the improvement is greater for the PAE at the lower frequency edge, as the points for optimum PAE is further from the centre in Figure 4.5.

5
Discussion

Below, other aspects of the presented results are discussed. This is done by first considering what sources of error that were present in the results, before ending by discussing future works and continuations of this project.

5.1 Sources of Error

The greatest source of error in this work should be considered to be the setup for the measurements. The initial plan was to order and measure on a PCB which had small distances between each components, had been run through a simulator and had its own calibration kits. It was also certain that the distance between amplifier and hybrid was the same for both the upper and lower amplifier, meaning that no extra imbalance in phase was introduced. However, as the PCB had a longer ordering time than expected, a makeshift measuring setup was used. This meant that the risk of phase- and amplitude imbalance was greater and that there were more interfaces which could introduce losses or reflections into the system. For a full description of the design of the PCB, see appendix C.

Though, while measuring on the system there was no observation of great reflections or a poor performance of the balancing of the amplifier. Hence, the indications of the results could be considered valid although the exact numbers presented should not be taken as a true result.

Another source of error in the results could be the extent of the simulations. With more time available or access to a more rigid simulation device, the extent of the simulations could be made more precise. This could be done through more points in the simulation or by solving the problem of the oscillating circuit in some other way than introducing attenuators in the circuit. However, as discussed above, these simulation were more of an indication of the validity of the theoretical equation. For this purpose, the simulations should be considered sufficient.

5.2 Future Works

In order to determine the exact extent of the improvement gained by load modulation, more precise measurements should be done. Preferably by using a PCB which is designed specifically for this purpose, for example the PCB which was designed for this work. One could also monitor the output power for each of the amplifiers individually to see if they truly do have different operating conditions. The analysis could be further developed by then examining the impact of amplitude- and phase imbalance in the system in order to compare that work with this report. The measurements could also be done for different amplitudes of the control signal in order to find the optimum control signal for each of the topologies. Another continuation of this project could be to examine to which extent the bandwidth of the amplifier can be improved. Although this is not the main focus of load modulation, it could be of interest to see the full tunability of the amplifier. As the different topologies are further examined, they should be compared to previous works which offer other solutions to matching errors. For example using varactors as impedance tuners [22], p-i-n diodes [23] or switches in order to reconfigure the matching networks of the circuit [24].

As a way of implementing the LMBA in a radar system, a slightly different setup could be used. A method which is used in some radar systems is to characterise the system at first, and then tune it digitally for different operating conditions or to compensate for different lengths of cables, among other things. If the reflections of an AESA could be characterised and predicted beforehand, a digital phase shifter could be used to control the phase of the control signal depending on the steering angle. This would mean that for each steering angle, the amplifiers would operate optimally and the AESA would perform better However, this digital phase shifter would probably consume some amount of power, which should be taken into consideration when calculating the PAE.

6
Conclusions

This work assesses whether or not there is a way to compensate for reflections due to coupling between antenna elements or a mismatched output of a system. These reflections changes the operational point of the amplifier and in turn, it also changes its characteristics, possibly yielding lower output power or worsened efficiency. The solutions that are in place today are often bulky or hard to integrate, meaning that a compensating system could play an important role in today's communication- and radar solutions. This report focuses on using the LMBA and its various topologies in order to solve this issue.

Initially, the theory behind reflections in an AESA is presented in order to show that these are dependent on the coupling between antenna elements and the steering angle of the antenna. Then, the load modulation of the LMBA is analysed. This part focuses on explaining how the control signal moves the load experienced by the amplifier by plotting these in a Smith chart. The analysis is done by calculating the S-matrices of the different topologies, the BA, LMBA, OLMBA, RLMBA and RefLMBA, and then creating plots for the matched- and unmatched cases in Smith charts. It is shown that there are ways to compensate for reflections in the system, but that it is difficult to compensate both of the amplifiers at the same time. Although, the RefLMBA shows some advantage as it is not being load modulated in the matched case and having its reflection coefficients close to the centre of the Smith chart in the unmatched case. It also indicates that in order to compensate for the reflections, the shift of the control signal has to be actively tuned in order to optimize the performance of the amplifiers.

Then, the reflection coefficients are verified by simulating the circuits using ADS. While some discrepancies occur, the general characteristics of each of the topologies are verified. Then, a makeshift BA is built and measured upon in order to further verify the theory. It clearly confirms the principle of load modulation, as the output power and PAE both are affected by the control signal and there is no precise correlation between these two figures of merits. It also shows that the phase of the control signal has to be actively controlled in order to enhance the performance of the amplifiers and compensate for the reflections. However, it is clear that it is possible to use this technique for compensation.

As a continuation of this work, the LMBA topologies presented here should be examined using a PCB designed specifically for this work. As this reduced the amplitude- and phase imbalance, as well as the losses due to interfaces in the circuits, it should give a more precise result than that of this report. One should also monitor the output power of each amplifier in order to verify that they truly operate differently. Another way forward could be to first characterise a system and its reflections, and then build a circuitry that chooses the correct shift of the control signal for each case. If such a system were to be built, it would remove the need for isolators or circulators while increasing the output power or PAE of the system.

Bibliography

[1] S. AB, "Aesa: A sensor suite for advanced threats," 2020. https://www.saab.com/markets/india/gripen-for-india/technology/aesa-a-sensor-suite-for-advanced-threats, [2024-05-08].

[2] D.-T. Huynh, M. Chen, T.-T. Huynh, and C. H. Hai, "Energy consumption optimization for green device-to-device multimedia communications," *Future Generation Computer Systems*, vol. 92, pp. 1131–1141, 2019.

[3] D. M. Pozar, *Microwave and RF design of wireless systems*. John Wiley & Sons, 2000.

[4] M. Mehrpoo, B. Patra, J. Gong, J. van Dijk, H. Homulle, G. Kiene, A. Vladimirescu, F. Sebastiano, E. Charbon, and M. Babaie, "Benefits and challenges of designing cryogenic cmos rf circuits for quantum computers," pp. 1–5, 2019.

[5] A. Sheikhi, "Historical aspect of load-modulated balanced amplifiers," *IEEE Access*, 2024.

[6] D. J. Shepphard, J. Powell, and S. C. Cripps, "An efficient broadband reconfigurable power amplifier using active load modulation," *IEEE Microwave and Wireless Components Letters*, vol. 26, no. 6, pp. 443–445, 2016.

[7] R. J. Mailloux, *Phased array antenna handbook*. Artech house, 2017.

[8] S. AB, "Our product areas," 2024. https://www.saab.com/products, [2024-05-15].

[9] UN, "Peace and security," 2024. https://www.un.org/en/global-issues/peace-and-security, [2024-05-16].

[10] E. Gelenbe, "Electricity consumption by ict: Facts, trends, and measurements," *Ubiquity*, vol. 2023, no. August, pp. 1–15, 2023.

[11] M. Attaran, "The impact of 5g on the evolution of intelligent automation and industry digitization," *Journal of ambient intelligence and humanized computing*, vol. 14, no. 5, pp. 5977–5993, 2023.

[12] A. D. Brown, *Active electronically scanned arrays: fundamentals and applications*. John Wiley & Sons, 2021.

[13] D. M. Pozar, "A relation between the active input impedance and the active element pattern of a phased array," *IEEE Transactions on Antennas and Propagation*, vol. 51, no. 9, pp. 2486–2489, 2003.

[14] C. Fager, K. Hausmair, K. Buisman, K. Andersson, E. Sienkiewicz, and D. Gustafsson, "Analysis of nonlinear distortion in phased array transmitters," in *2017 Integrated Nonlinear Microwave and Millimetre-wave Circuits Workshop (INMMiC)*, pp. 1–4, IEEE, 2017.

[15] R. Navarathna, D. T. Le, A. R. Hamann, H. D. Nguyen, T. M. Stace, and A. Fedorov, "Passive superconducting circulator on a chip," *Physical review letters*, vol. 130, no. 3, p. 037001, 2023.

[16] F. M. Ghannouchi and M. S. Hashmi, *Load-pull techniques with applications to power amplifier design*, vol. 32. Springer Science & Business Media, 2012.

[17] T. Yuan, R. Quaglia, K. Chaudhry, E. Azad, J. R. Powell, and S. C. Cripps, "Output signal re-injection in load-modulated balanced amplifiers for rf bandwidth improvement," *IEEE Microwave and Wireless Technology Letters*, 2023.

[18] R. Quaglia, J. R. Powell, K. A. Chaudhry, and S. C. Cripps, "Mitigation of load mismatch effects using an orthogonal load modulated balanced amplifier," *IEEE Transactions on Microwave Theory and Techniques*, vol. 70, no. 6, pp. 3329–3341, 2022.

[19] D. J. Collins, R. Quaglia, J. R. Powell, and S. C. Cripps, "The orthogonal lmba: A novel rfpa architecture with broadband reconfigurability," *IEEE Microwave and Wireless Components Letters*, vol. 30, no. 9, pp. 888–891, 2020.

[20] Anaren, "Model xc3500m-03s," 2018. https://www.mouser.com/datasheet/2/21/XC3500M-03S_DataSheet(Rev_B)-1221769.pdf, [2024-05-08].

[21] Anaren, "Ultra low profile 0805 10db directional coupler," 2022. https://www.mouser.se/datasheet/2/21/DC2337J5010AHF-3364618.pdf, [2024-05-24].

[22] C. Sánchez-Pérez, C. M. Andersson, K. Buisman, D. Kuylenstierna, N. Rorsman, and C. Fager, "Design and large-signal characterization of high-power varactor-based impedance tuners," *IEEE Transactions on Microwave Theory and Techniques*, vol. 66, no. 4, pp. 1744–1753, 2018.

[23] J. De Mingo, A. Valdovinos, A. Crespo, D. Navarro, and P. Garcia, "An rf electronically controlled impedance tuning network design and its application to an antenna input impedance automatic matching system," *IEEE Transactions on Microwave Theory and Techniques*, vol. 52, no. 2, pp. 489–497, 2004.

[24] A. van Bezooijen, M. A. De Jongh, C. Chanlo, L. C. Ruijs, F. van Straten, R. Mahmoudi, and A. H. van Roermund, "A gsm/edge/wcdma adaptive series-lc matching network using rf-mems switches," *IEEE Journal of Solid-State Circuits*, vol. 43, no. 10, pp. 2259–2268, 2008.

[25] I. group, "I-tera mt40," 2024. https://www.isola-group.com/pcb-laminates-prepreg/i-tera-mt40/, [2024-05-08].

[26] G. Kim and S. Kim, "Design and analysis of dual polarized broadband microstrip patch antenna for 5g mmwave antenna module on fr4 substrate," *IEEE Access*, vol. 9, pp. 64306–64316, 2021.

[27] Keysight, "Keysight vna series network analyzers," 2024. https://www.keysight.com/gb/en/assets/9018-07786/user-manuals/9018-07786.pdf?success=true, [2024-05-09].

A

MATLAB Code

Below is the used MATLAB code presented.

A.1 Frequency Sweep

```
%% Program for sweeping power and find correct operational point
% First: Factory preset for all instruments
% Also: declare filename. This will be used to save the workspace
    and the S-parameters
clf
close all
clear all
% Open and reset all
ENA('open');
ENA('factory_preset')
AFG31000('open');
AFG31000('reset');
HP6643A_VD('open');
HP6643A_VD('reset')
HP6643A_PREAMP('open')
HP6643A_PREAMP('reset')

dialogfields = {'Enter file name (TOPOLOGY_POWERSWEEP_EXTRA):'};
dialogtitle = 'Input:';
dialogdimensions = [1 45];
defaultinput = {'LMBA_POWERSWEEP_INTEGRATED'};
answer = inputdlg(dialogfields,dialogtitle, dialogdimensions,
    defaultinput);
filename = answer{1};

%% Open Vg, specify its characteristics
Vg1_high = -3;      % [V], search for 1.1A
Vg_low = -5.5;      % [V]
Vg2_high = -3;      % [V], search for 1.1A
Vg_period = 100e-6; % [s]
Vg_duty = 10;       % [%]
AFG31000('open');
% Pulse shape
AFG31000('write', 'SOUR1:FUNC:SHAPE PULSE')
AFG31000('write', 'SOUR2:FUNC:SHAPE PULSE')
% High Z output
AFG31000('write', 'OUTPUT1:IMPEDANCE INF')
AFG31000('write', 'OUTPUT2:IMPEDANCE INF')
% Below: Set values for function generator
```

```
38 AFG31000('set_low','1',num2str(Vg_low))
39 AFG31000('set_low','2',num2str(Vg_low))
40 AFG31000('set_high','1',num2str(Vg1_high))
41 AFG31000('set_high','2',num2str(Vg2_high))
42 AFG31000('period','1',num2str(Vg_period))
43 AFG31000('period','2',num2str(Vg_period))
44 AFG31000('duty_cycle','1',num2str(Vg_duty))
45 AFG31000('duty_cycle','2',num2str(Vg_duty))
46 AFG31000('RF1_on')
47 AFG31000('RF2_on')
48 disp(['Duty cycle set to ' num2str(Vg_duty) '%'])
49 disp(['Period set to ' num2str(Vg_period) 's'])
50 disp(['Low set to ' num2str(Vg_low) 'V, high set to ' num2str(
       Vg1_high) ' V and ' num2str(Vg2_high) 'V'])
51
52 %% Open Vpreamp, specify its characteristics
53 Vpreamp = 28;      % [V]
54 imaxpreamp = 3000;% [mA]
55 HP6643A_PREAMP('open');
56 HP6643A_PREAMP('vset', [num2str(Vpreamp) 'V'])
57 % Over current protection
58 HP6643A_PREAMP('ocp', num2str(imaxpreamp))
59 HP6643A_PREAMP('on')
60 disp(['V_preamp set to ' num2str(Vpreamp) 'V'])
61
62 %% Open Vd, specify its characteristics
63 Vd = 30;        % [V]
64 imaxvd = 3000; % [mA]
65 HP6643A_VD('open');
66 HP6643A_VD('vset', [num2str(Vd) 'V'])
67 % Over current protection
68 HP6643A_VD('ocp', num2str(imaxvd))
69 HP6643A_VD('on')
70 disp(['Vd set to ' num2str(Vd) 'V'])
71
72 %% Characterise ENA
73 P_in = -1;                                          % [dBm]
74 f_start = 10e6;                                     % [Hz]
75 f_stop = 12e9;
76 num_points = 1000;
77 ena_delay = 1e-6;                                   % [s]
78 ena_width = 0.01*Vg_duty*Vg_period-3*ena_delay;% [s]
79 ENA('open');
80 ENA('power_off')
81 % Initiate windows
82 ENA('write','DISP:WIND1 ON')
83 ENA('write','CALC:MEAS1:DEF "S11"')
84 ENA('write','DISP:WIND1:TRAC1:FEED:MNUMBER 1')
85 ENA('write','DISP:WIND2 ON')
86 ENA('write','CALC:MEAS2:DEF "S21"')
87 ENA('write','DISP:WIND2:TRAC1:FEED:MNUMBER 2')
88 ENA('write','DISP:WIND3 ON')
89 ENA('write','CALC:MEAS3:DEF "S31"')
90 ENA('write','DISP:WIND3:TRAC1:FEED:MNUMBER 3')
91 ENA('write','DISP:WIND4 ON')
92 ENA('write','CALC:MEAS4:DEF "S41"')
```

```
93  ENA('write','DISP:WIND4:TRAC1:FEED:MNUMBER 4')
94  % Load cal set "Luddes"
95  ENA('write','SENSE:CORRECTION:CSET:ACTIVATE "Luddes", ON')
96  % Sets sweep type to linear frequency
97  ENA('write', 'SENS:SWE:TYPE LIN')
98  % Set starting frequency
99  ENA('write', ['SENSE:FREQ:START ' num2str(f_start)])
100 % Set upper limit for frequency
101 ENA('write', ['SENSE:FREQ:STOP ' num2str(f_stop)])
102 % Set Power
103 ENA('write', ['SOURCE:POWER:LEVEL ' num2str(P_in)])
104 % Set number of swept points
105 ENA('write', ['SENS:SWEEP:POIN ' num2str(num_points)])
106 % Turns on pulse modulation
107 ENA('write', 'SOURCE:PULSE:MODULATOR ON')
108 % Pulse from external source
109 ENA('write', 'SENS:SWE:PULS:PRIM:CLOC "External"')
110 % Autoselect Profile Sweep Time ON
111 ENA('write', 'SENS:SWE:PULS:CWT ON')
112 % Autoselect width and delay OFF
113 ENA('write', 'SENS:SWE:PULS:TIM OFF')
114 % External pulse trigger source
115 ENA('write', 'SENSE:PATH:CONFIG:ELEMENT "PulseTrigInput", "External
    "')
116 % Enable channel for external pulse
117 ENA('write', 'SENSE:SWE:PULS:DRIV ON')
118 % Set Pulse width
119 ENA('write', ['SENS:SWE:PULS:MAST:WIDTH ' num2str(0.01*Vg_duty*
    Vg_period)])
120 % Set pulse period
121 ENA('write', ['SENS:SWE:PULS:MAST:PER ' num2str(Vg_period)])
122 % Set measurement timing width
123 ENA('write', ['SENSE:PULSE:WIDTH ' num2str(ena_width)])
124 % Set measurement timing delay
125 ENA('write', ['SENSE:PULSE:DELAY ' num2str(ena_delay)])
126 % Pulse trigger on edge
127 ENA('write', 'SENS:PULSE:TTYP EDGE')
128 % Positive polarity on pulse trigger
129 ENA('write', 'SENS:PULS:TPOL POS')
130 % Enable synchronize adcs using pulse trigger
131 ENA('write','SENSE:PULSE0 1')
132 % Define STD
133 ENA('write', 'SENS:SWE:PULS:MODE STD')
134
135 ENA('power_on')
136
137 sweep_time = 5 + Vg_period*num_points*1.1;
138 disp('Measuring...')
139 % Wait while measurements are done, Ctrl + C to abort
140 pause(round(sweep_time))
141 disp('Done!')
142
143 %% Save workspace and Data to s4p
144 ENA('make_get_s2p',[filename '.s4p'],['C:\Users\u095839\Desktop\
    Master Thesis\Matlab\' filename '.s4p'])
145 save([filename,'.mat'])
```

```
%% Close instruments
ENA('power_off')
pause(1)
HP6643A_VD('off')
pause(1)
HP6643A_PREAMP('off')
pause(1)
AFG31000('RF1_off')
AFG31000('RF2_off')
```

A.2 Power Sweep

```
%% Program for sweeping power and find correct operational point
% First: Factory preset for all instruments
% Also: declare filename. This will be used to save the workspace
    and the S-parameters
clf
close all
clear all
ENA('open');
ENA('factory_preset')
AFG31000('open');
AFG31000('reset');
HP6643A_VD('open');
HP6643A_VD('reset')
HP6643A_PREAMP('open')
HP6643A_PREAMP('reset')


dialogfields = {'Enter file name (TOPOLOGY_POWERSWEEP_EXTRA):'};
dialogtitle = 'Input:';
dialogdimensions = [1 45];
defaultinput = {'LMBA_POWERSWEEP_INTEGRATED'};
answer = inputdlg(dialogfields,dialogtitle, dialogdimensions,
    defaultinput);
filename = answer{1};

%% Open Vg, specify its characteristics
Vg1_high = -3;      % [V]
Vg_low = -5;        % [V]
Vg2_high = -3;      % [V]
Vg_period = 100e-6;% [s]
Vg_duty = 10;       % [%]
AFG31000('open');
% Pulse shape
AFG31000('write', 'SOUR1:FUNC:SHAPE PULSE')
AFG31000('write', 'SOUR2:FUNC:SHAPE PULSE')
% High Z output
AFG31000('write', 'OUTPUT1:IMPEDANCE INF')
AFG31000('write', 'OUTPUT2:IMPEDANCE INF')
AFG31000('set_low','1',num2str(Vg_low))
AFG31000('set_low','2',num2str(Vg_low))
AFG31000('set_high','1',num2str(Vg1_high))
AFG31000('set_high','2',num2str(Vg2_high))
AFG31000('period','1',num2str(Vg_period))
AFG31000('period','2',num2str(Vg_period))
```

```
43 AFG31000('duty_cycle','1',num2str(Vg_duty))
44 AFG31000('duty_cycle','2',num2str(Vg_duty))
45 AFG31000('RF1_on')
46 AFG31000('RF2_on')
47 disp(['Duty cycle set to ' num2str(Vg_duty) '%'])
48 disp(['Period set to ' num2str(Vg_period) 's'])
49 disp(['Low set to ' num2str(Vg_low) 'V, high set to ' num2str(
       Vg1_high) ' V and ' num2str(Vg2_high) 'V'])
50
51 %% Open Vpreamp, specify its characteristics
52 Vpreamp = 28; % [V]
53 imax = 3000;  % [mA]
54 HP6643A_PREAMP('open');
55 HP6643A_PREAMP('vset', [num2str(Vpreamp) 'V'])
56 HP6643A('ocp', num2str(imax))
57 HP6643A_PREAMP('on')
58 disp(['V_preamp set to ' num2str(Vpreamp) 'V'])
59
60 %% Open Vd, specify its characteristics
61 Vd = 30;      % [V]
62 imax = 3000; % [mA]
63 HP6643A_VD('open');
64 HP6643A_VD('vset', [num2str(Vd) 'V'])
65 HP6643A_VD('ocp', num2str(imax))
66 HP6643A_VD('on')
67 disp(['Vd set to ' num2str(Vd) 'V'])
68
69 %% Characterise ENA
70 P_start = -30;                                    % [dBm]
71 P_stop = 10;                                      % [dBm]
72 f = 3e9;                                          % [Hz]
73 num_points = 1000;
74 ena_delay = 1e-6;                                 % [s]
75 ena_width = 0.01*Vg_duty*Vg_period-3*ena_delay;% [s]
76 ENA('open');
77 ENA('power_off')
78 % Initiate windows
79 ENA('write','DISP:WIND1 ON')
80 ENA('write','CALC:MEAS1:DEF "S11"')
81 ENA('write','DISP:WIND1:TRAC1:FEED:MNUMBER 1')
82 ENA('write','DISP:WIND2 ON')
83 ENA('write','CALC:MEAS2:DEF "S21"')
84 ENA('write','DISP:WIND2:TRAC1:FEED:MNUMBER 2')
85 ENA('write','DISP:WIND3 ON')
86 ENA('write','CALC:MEAS3:DEF "S31"')
87 ENA('write','DISP:WIND3:TRAC1:FEED:MNUMBER 3')
88 ENA('write','DISP:WIND4 ON')
89 ENA('write','CALC:MEAS4:DEF "S41"')
90 ENA('write','DISP:WIND4:TRAC1:FEED:MNUMBER 4')
91 % Load cal set "Luddes"
92 ENA('write','SENSE:CORRECTION:CSET:ACTIVATE "Luddes", ON')
93 % Sets sweep type to power
94 ENA('write', 'SENS:SWE:TYPE POW')
95 % Set starting power
96 ENA('write', ['SOURCE:POWER:START ' num2str(P_start)])
97 % Set upper limit for power
```

```
98  ENA('write', ['SOURCE:POWER:STOP ' num2str(P_stop)])
99  % Set frequency
100 ENA('write', ['SENS:FREQ:FIX ' num2str(f)])
101 % Set number of swept points
102 ENA('write', ['SENS:SWEEP:POIN ' num2str(num_points)])
103 % Turns on pulse modulation
104 ENA('write', 'SOURCE:PULSE:MODULATOR ON')
105 % Pulse from external source
106 ENA('write', 'SENS:SWE:PULS:PRIM:CLOC "External"')
107 % Autoselect Profile Sweep Time ON
108 ENA('write', 'SENS:SWE:PULS:CWT ON')
109 % Autoselect width and delay OFF
110 ENA('write', 'SENS:SWE:PULS:TIM OFF')
111 %External pulse trigger source
112 ENA('write', 'SENSE:PATH:CONFIG:ELEMENT "PulseTrigInput", "External
    "')
113 % Enable channel for external pulse
114 ENA('write', 'SENSE:SWE:PULS:DRIV ON')
115 % Set Pulse width
116 ENA('write', ['SENS:SWE:PULS:MAST:WIDTH ' num2str(0.01*Vg_duty*
    Vg_period)])
117 % Set pulse period
118 ENA('write', ['SENS:SWE:PULS:MAST:PER ' num2str(Vg_period)])
119 % Set measurement timing width
120 ENA('write', ['SENSE:PULSE:WIDTH ' num2str(ena_width)])
121 % Set measurement timing delay
122 ENA('write', ['SENSE:PULSE:DELAY ' num2str(ena_delay)])
123 % Pulse trigger on edge
124 ENA('write', 'SENS:PULSE:TTYP EDGE')
125 % Positive polarity on pulse trigger
126 ENA('write', 'SENS:PULS:TPOL POS')
127 % Enable synchronize adcs using pulse trigger
128 ENA('write','SENSE:PULSE0 1')
129 % Define STD
130
131 ENA('write', 'SENS:SWE:PULS:MODE STD')
132 ENA('power_on')
133
134 sweep_time = 5 + Vg_period*num_points*1.1;
135 disp('Measuring...')
136 pause(round(sweep_time)) % Ctrl + C to abort
137 disp('Done!')
138
139 %% Save workspace and Data to s4p
140 ENA('make_get_s2p',[filename '.s4p'],['C:\Users\u095839\Desktop\
    Master Thesis\Matlab\' filename '.s4p'])
141 save([filename,'.mat'])
142 %% Close instruments
143 ENA('power_off')
144 pause(1)
145 HP6643A_VD('off')
146 pause(1)
147 HP6643A_PREAMP('off')
148 pause(1)
149 AFG31000('RF1_off')
150 AFG31000('RF2_off')
```

B

Setups for DUTs

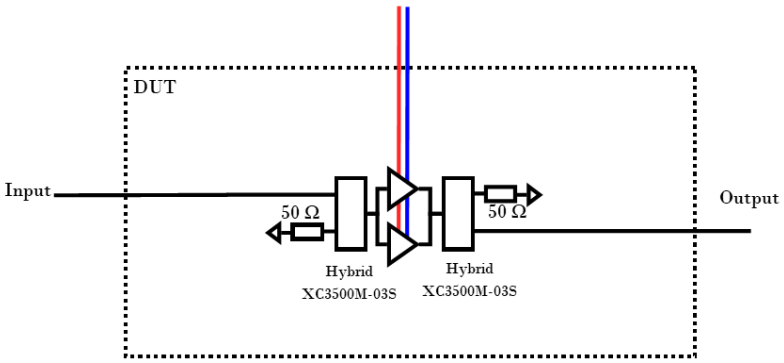

Figure B.1: The DUT setup for the BA measurements. For the complete setup see Figure 3.2

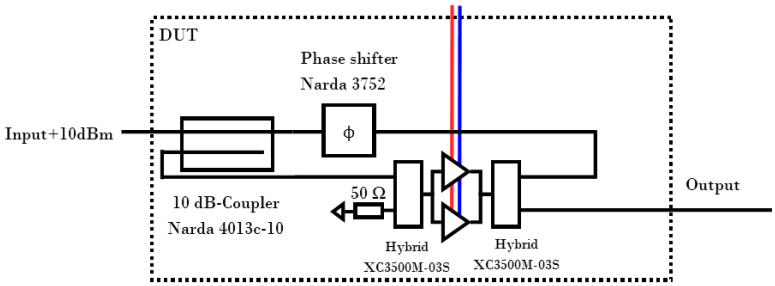

Figure B.2: The DUT setup for the LMBA measurements. For the complete setup, see Figure 3.2

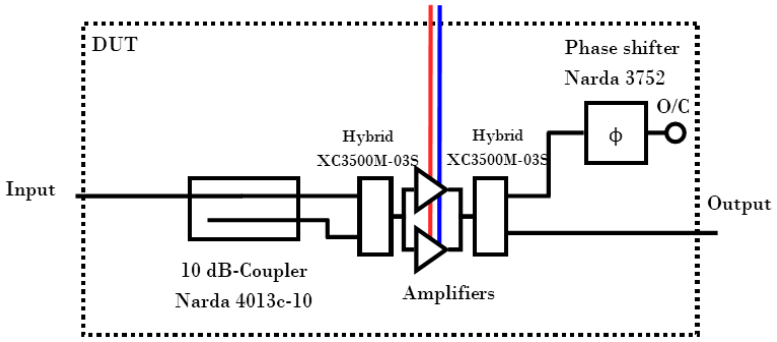

Figure B.3: The DUT setup for the OLMBA measurements. For the complete setup, see Figure 3.2

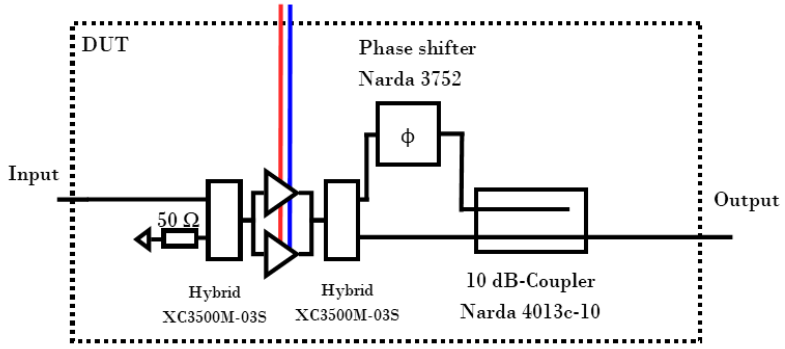

Figure B.4: The DUT setup for the RLMBA measurements. For the complete setup, see Figure 3.2

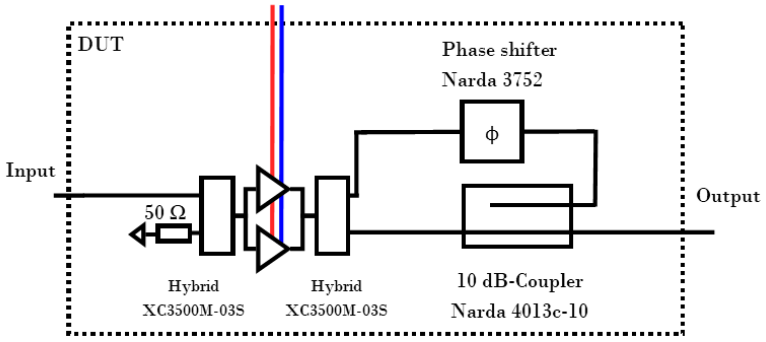

Figure B.5: The DUT setup for the RefLMBA measurements. For the complete setup, see Figure 3.2

C
Design

When designing the PCB used for testing the circuits, Cadence Allegro was used. This began by drawing a circuit diagram of all of the circuits that were going to be on the PCB. Then, the logic and all of the footprints from the circuit diagram were imported into Cadence Allegro. In accordance with the limitations set for this thesis work, components were picked that resulted in the fastest ordering- and design time. This meant that it was beneficial to use components which already existed in Saab's system, as this meant that all of the footprints already were drawn. The values for components such as capacitances that were used in the biasing network were copied from previous work with this specific amplifier that had been rigorously measured upon. A complete list of the components that were used can be found in Table C.1 below. The full circuit diagrams can be found in Appendix D.

Table C.1: The components used in the design of the PCB.

Part	**Name**	**Part**	**Name**
90° Hybrid	XC3500M-03S	Headers	146131-4
10 dB-coupler	DC2337J5010AHF	220 µF	UCD1H221MNL1GS
Rosenberger contact	02K80A-40ML5	47 pF	06035A470JAT2A
50 Ω, 8 W	C8A50Z4B	330 pF	06035A331JAT2A
51 Ω, 0.125 W	RK73H1JTTD51R0F	1 nF	06035A102JAT2A
		10 nF	CC0603JRNPO9BN103

Then, the PCB was drawn. This began by defining the dielectric material to be used as well as its thickness and the thickness of the conductors. These parameters were then put into the simulation tool 'LineCalc' in ADS, which calculated the required width of the conductors in order to obtain a 50 Ω transmission line. The dielectric chosen was 254 µm, or 10 mil, thick I-Tera MT40, which has a dielectric constant of $\epsilon_r = 3.45$ [25]. As the thickness of the conductors was chosen to be 17 µm, the resulting width of the transmission lines was calculated to 560 µm at 3 GHz. This width was close to the width of the Rosenberger footprint as well as the pads of the quad flat no-lead package (QFN) which the amplifier was packages in. This is beneficial as it minimizes the losses from tapering needed to connect to these components. Initially, the PCB was going to be built of four conducting layers, where the middle dielectric would be thicker in order to make the PCB more durable. However, in order to match the transmission lines to the hybrids and 50 Ω, 8 W resistances, two extra layers were added. This was due to the fact that these were characterised on a thicker dielectric with another dielectric constant and hence had larger pads. In the data sheet of the hybrids [20], the manufacturer recommended matching the parasitic capacitances to the case in the data sheet. One proposed way of doing this was to open up the second layer under the pad, changing the capacitance C between layers. The thickness needed for the second dielectric layer was calculated using $C = \epsilon A/d$, where A was the area of the pad and d the distance between layers. This resulted in a second layer of I-Tera MT40 with thickness 508 µm or 20 mil. As the PCB structure need to be symmetric in order to avoid twisting and have an even number of conducting layers, a layer of FR-4 was added as a middle layer to increase stability. This material

was chosen for its low cost and common applications [26] and the manufacturer suggest that its thickness should be 274 µm in order for the total board thickness to be 1900 µm. The complete layer structure of the PCB can be seen in Figure C.1, where the precision was chosen in accordance with Saab's standards. All holes were chosen to have a diameter of 300 µm and a plating with a diameter of 650 µm.

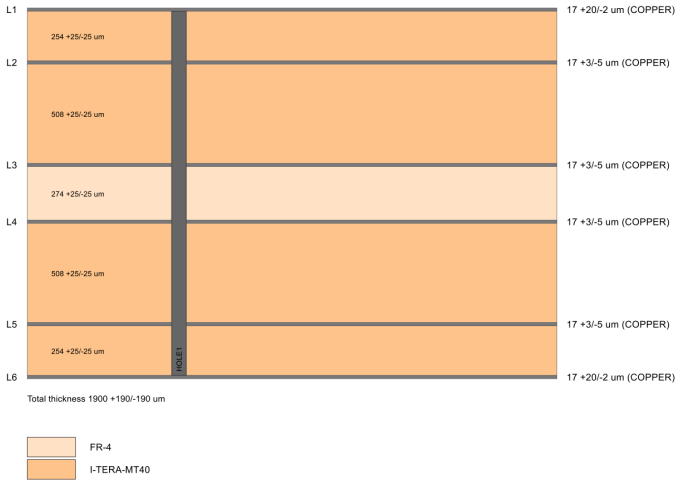

Figure C.1: A full view of the layer structure of the designed PCB.

As the structure of the PCB was finished, the placement and connecting of components was initiated. In this part, the focus lied on minimizing the lengths of the conductors between the amplifiers and the hybrids as well as the distances between the capacitances in the bias lines and the amplifier. This was done in order to minimize unwanted parasitics created by the transmission lines. One complication that arose was that the Rosenberger contacts were too wide to feed the hybrids from the direction that was needed. Hence some of the structures has bent transmission lines into the circuit. Because of this, a calibration kit (cal kit) with bent lines was added, apart from the cal kit with straight lines. The cal kits were of the type 'Through, Reflect, Line' (TRL), and contained one through circuit and one open circuit. Apart from these, two calibration circuits were designed for the desired frequency spectrum. The phase shift of the frequencies in these 'Line' measurement should lie between 20° and 160°. This is in accordance with the VNA's specifications [27, p.372-375]. These phase shifts were verified by simulation in ADS and the final range for the longer circuit was 1-7.8 GHz and 7.8-58 GHz for the shorter circuit. A full view of the drawn PCB can be found in Figure C.2, where yellow letters are added for each of the designed blocks. In Table C.2, there is an explanation for each of the letter, describing what the circuits in each block are designed for.

Another component that was designed was a cooling plate. This was viewed as a safety precaution in order to further cool down the amplifier. The cooling plate was planned to be fastened through four mechanical holes which can be found on each block that contains an amplifier on the PCB, see Figure C.2. Furthermore, the cooling plate needed holes for the Rosenberger contacts. The cooling plate was manufactured in-house by the author by sawing, drilling and threading a leftover, aluminium plate to the dimensions 80x175x3 mm. Apart from the mentioned holes, one extra hole was put in each corner of the plate. This was done in order to fasten extenders which lifted the cooling plate off the ground, enabling more air to flow beneath the plate.

Table C.2: Explanation of each block in Figure C.2.

	Description
A	A balanced amplifier where the isolated port of the first hybrid is terminated. Designed for LMBA measurements.
B	A balanced amplifier where all ports are available for connection. Designed to be used for any topology or to monitor the isolated ports.
C	A balanced amplifier with an extra hybrid at the output. Designed for RLMBA measurements, where attenuators may be used to lower control signal and simulate different couplers.
D	A balanced amplifier where the input is connected to a 10 dB-coupler. Designed for OLMBA measurements.
E	A balanced amplifier. To be used to compare the results to the load modulated case.
F	Control circuit for a hybrid without the matching done by opening up the plane below its pins.
G	A single amplifier. To be used for comparison with the balanced and load modulated case.
H	Control circuit for a hybrid with the matching done by opening up the plane below its pins.
I	Control circuit for the 10 dB-coupler.
J	Cal kit for the straight transmission lines.
K	Control circuits for the different components used in the circuits, as well as the capacitances by the bias lines.
L	Cal kit for the bent transmission lines.

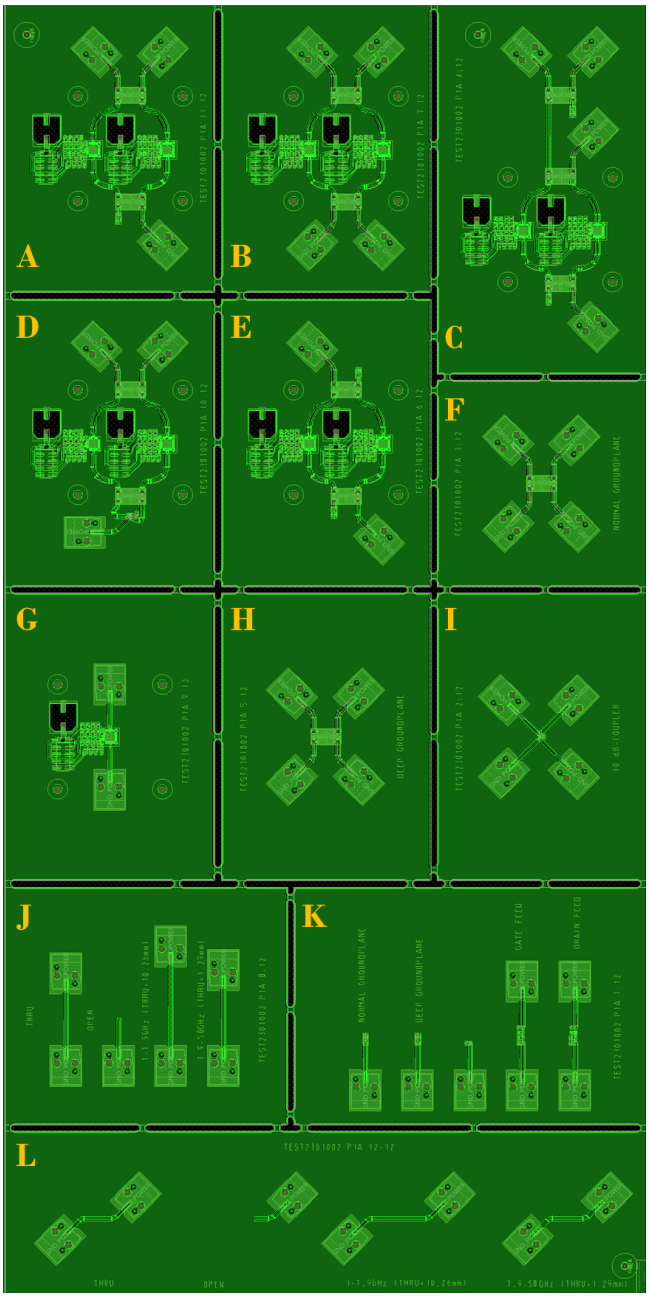

Figure C.2: Full drawing of the PCB, for explanation see Table C.2

D

Circuit Drawing

Below, the full circuit drawings for the designed PCB is shown. It should be noted that one circuit element may have multiple circuit symbols defined, which all have the same name. These are divided for the purpose to not make the circuit drawing too cluttered when many elements are included. However, all of the circuit symbols for each element is put on the same page.

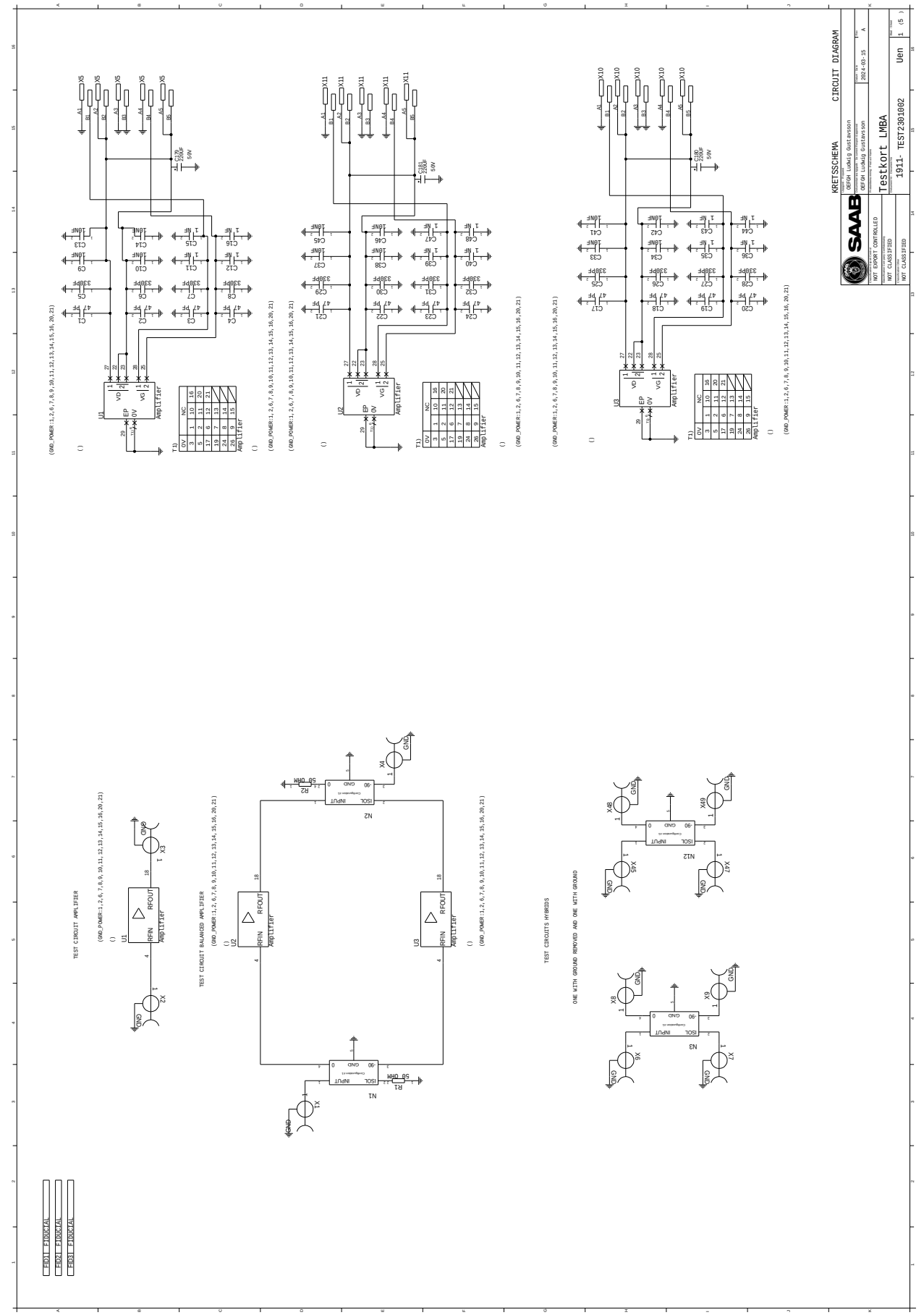
KRETSSCHEMA
CIRKUIT DIAGRAM
SAAB
OEFGH Ludvig Gustavsson
OEFGH Ludvig Gustavsson
2024-03-15
A
NOT EXPORT CONTROLLED
NOT CLASSIFIED
NOT CLASSIFIED
Testkort LMBA
1911- TEST2301002
Uen
1
(5)
TEST CIRCUIT AMPLIFIER
TEST CIRCUIT BALANCED AMPLIFIER
TEST CIRCUITS HYBRIDS
ONE WITH GROUND REMOVED AND ONE WITH GROUND
Amplifier
RFIN
RFOUT
VD
VG1
VG2
EP
0V
NC
GND
INPUT
ISOL
50 OHM

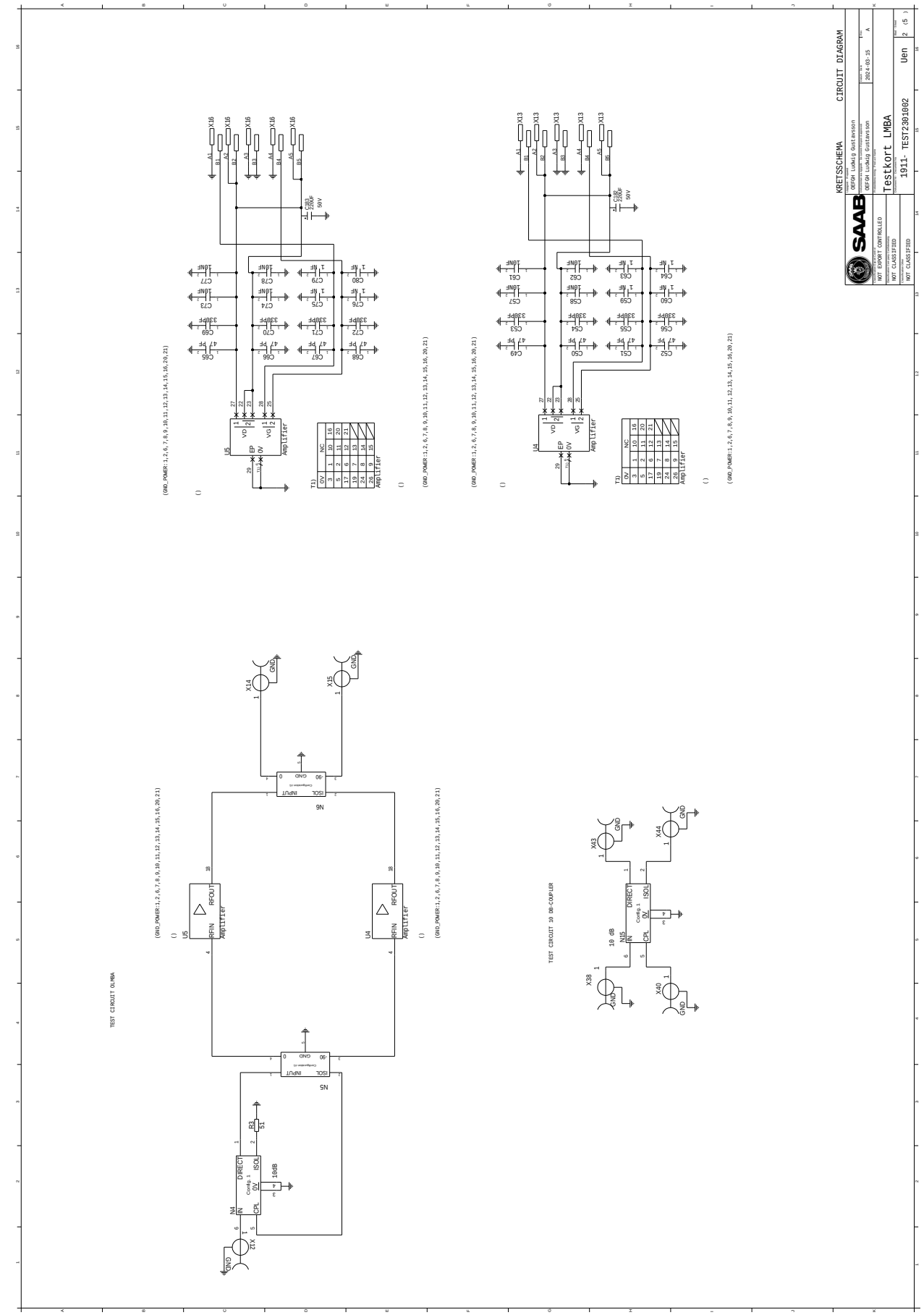
KRETSSCHEMA
CIRCUIT DIAGRAM
SAAB
OEFGH Ludvig Gustavsson
OEFGH Ludvig Gustavsson
2024-03-15
A
NOT EXPORT CONTROLLED
NOT CLASSIFIED
NOT CLASSIFIED
Testkort LMBA
1911- TEST2301002
Uen
2
TEST CIRCUIT LMBA
TEST CIRCUIT 10 DB-COUPLER
10 dB
GND
INPUT
ISOL
DIRECT
CPL
RFIN
RFOUT
AmpLifier

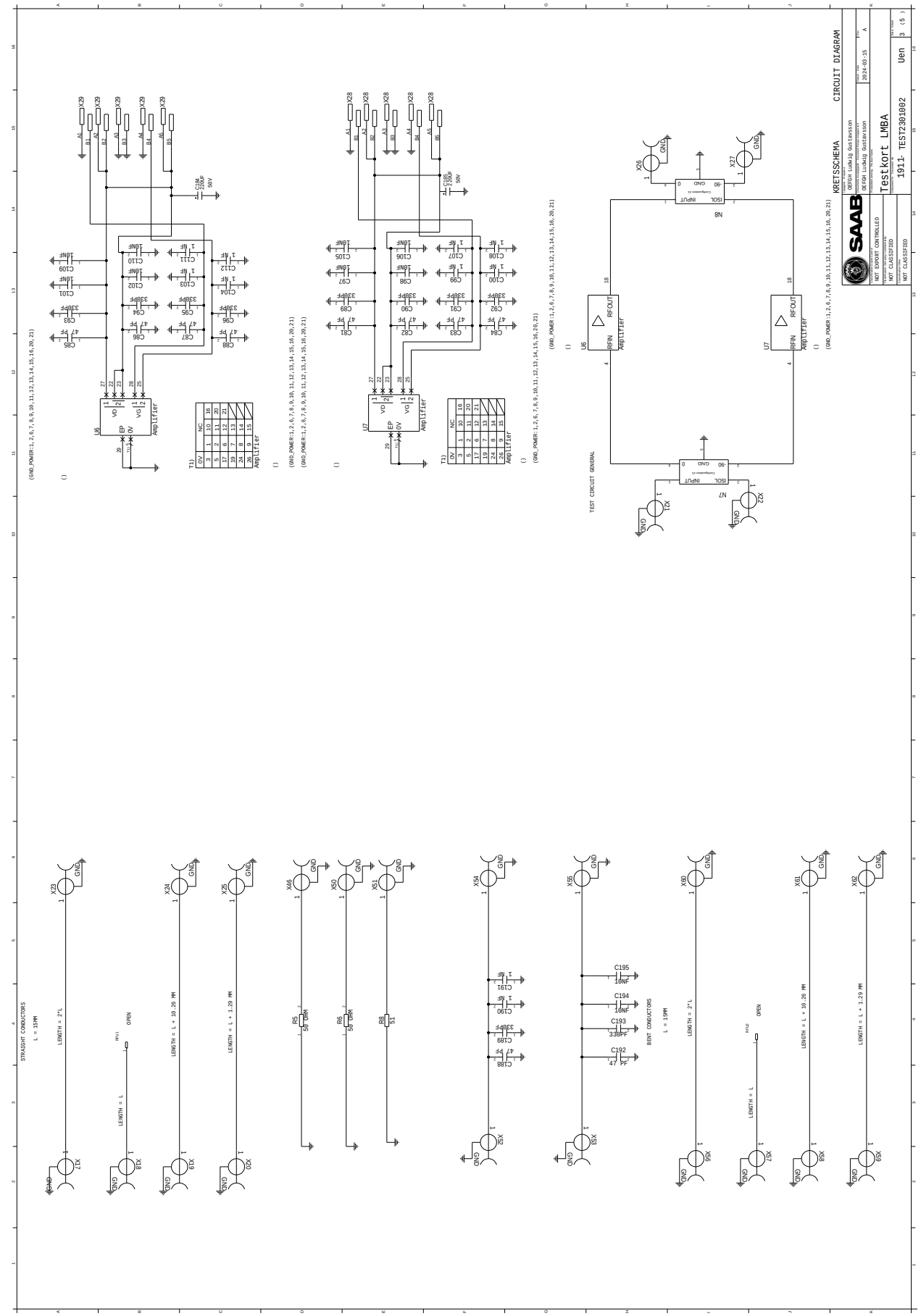
KRETSSCHEMA
CIRCUIT DIAGRAM
SAAB
Testkort LMBA
1911-TEST2301002
Uen
2024-03-15
NOT EXPORT CONTROLLED
NOT CLASSIFIED
TEST CIRCUIT GENERAL
STRAIGHT CONDUCTORS
L = 15MM
BENT CONDUCTORS
L = 15MM
Amplifier
RFIN
RF-OUT
INPUT
GND
OPEN

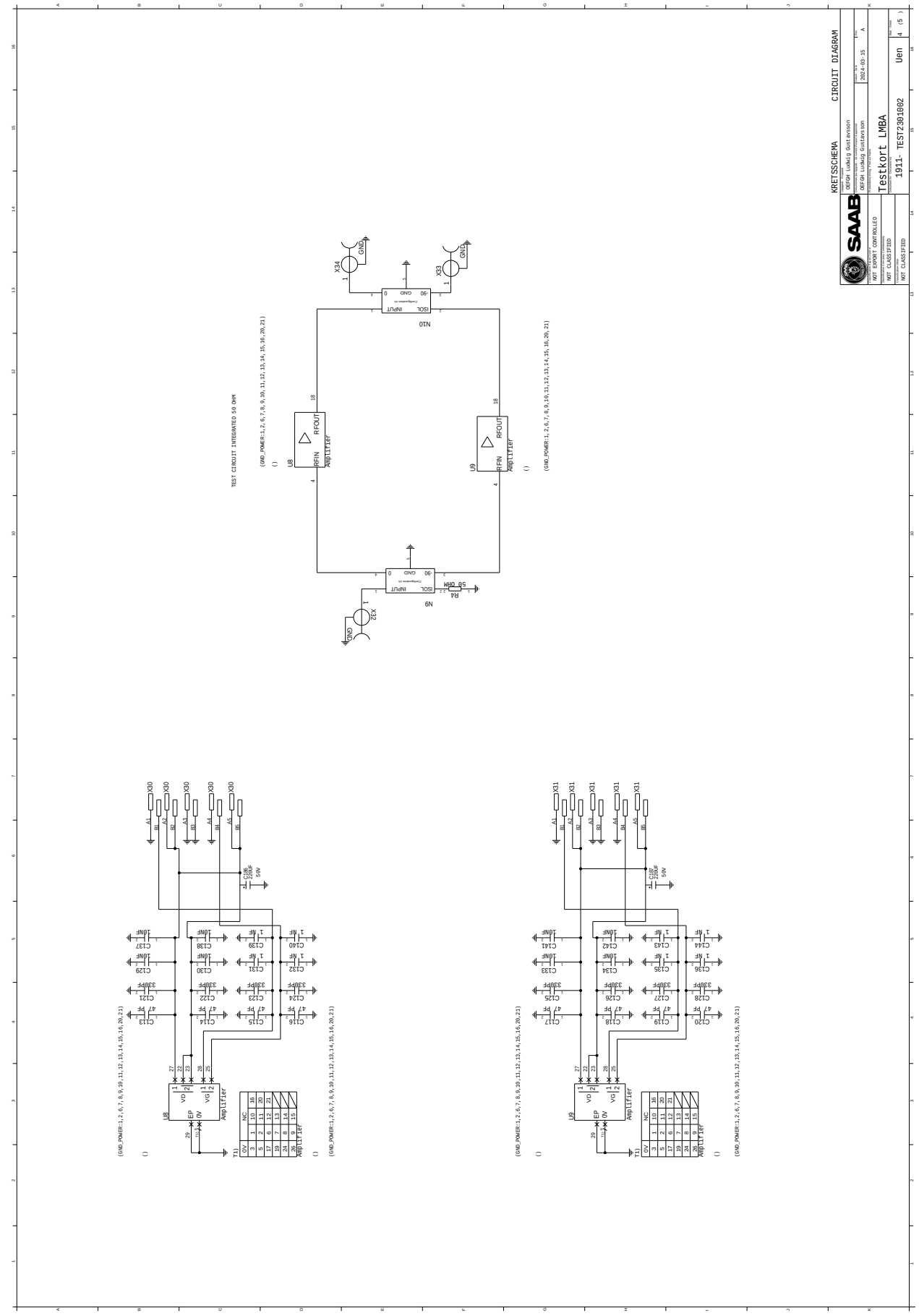
KRETSSCHEMA
CIRKUIT DIAGRAM
SAAB
OEFGH Ludwig Gustavsson
2024-08-15
NOT EXPORT CONTROLLED
NOT CLASSIFIED
Testkort LMBA
1911- TEST2301002
Uen
TEST CIRCUIT INTEGRATED 50 OHM
Amplifier
ISOL
INPUT
RFIN
RFOUT
GND
50 OHM

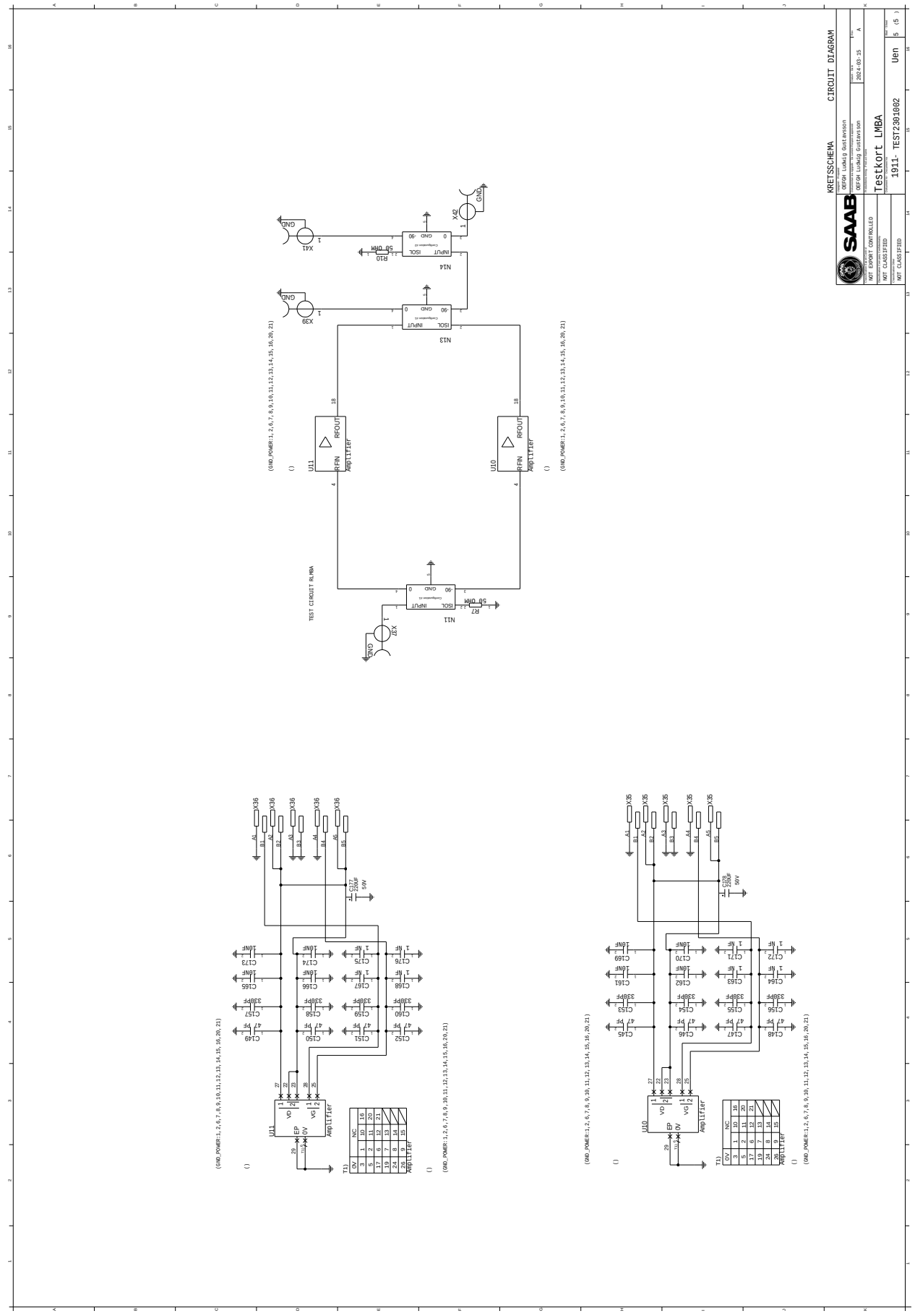
KRETSSCHEMA
CIRKUIT DIAGRAM
SAAB
OEFGH Ludwig Gustavsson
2024-03-15
A
NOT EXPORT CONTROLLED
NOT CLASSIFIED
Testkort LMBA
1911- TEST2301002
Uen
5
TEST CIRCUIT RLMBA
GND_POWER:1,2,6,7,8,9,10,11,12,13,14,15,16,20,21
Amplifier
RFOUT
RFIN
ISOL
INPUT
GND
50 OHM
10NF
1 NF
330PF
47 PF
220UF
50V
NC
0V
EP
VD
VG

DEPARTMENT OF MICROTECHNOLOGY AND NANOSCIENCE
CHALMERS UNIVERSITY OF TECHNOLOGY
Gothenburg, Sweden
www.chalmers.se

CHALMERS
UNIVERSITY OF TECHNOLOGY